中国创造学会

简报

2025年第6期
【总第39期】

2025年6月

☆通知公告☆

关于开展 2025 年“创新创业创造教育与拔尖创新人才培养”主题征文的通知

为深入学习贯彻党的二十大、二十届三中全会精神、习近平总书记《论教育》和新时代做好人才工作的重要思想，落实《教育强国建设规划纲要（2024—2035 年）》、2015 年国务院办公厅《关于深化高等学校创新创业教育改革的实施意见》精神，深刻领会习近平总书记关于创新创业创造重要论述的时代内涵，聚焦教育强国建设的拔尖创新人才培养国家战略，完善拔尖创新人才发现和培养机制，促进创新创业创造教育理论研究与实践发展，为中国式现代化建设提供有力的人才支撑，特开展本次征文活动。

详见网址：http://chinaccsis.com/Data/View/877

关于举办 2025 年“邯郸杯”全国青少年创语未来成语文化创新大赛的通知

为加强青少年学生对中国优秀传统文化的学习和研究，激励对成语文化的挖掘和热爱，激活成语文化的生命力，创新传承和弘扬优秀传统文化的媒介和路径，增强文化自信，经研究决定举办 2025 年（首届）“邯郸杯”全国青少年创语未来成语文化创新大赛。

详见网址：http://chinaccsis.com/Data/View/878

关于举办立达设计奖·第四届国际大学生校园设计大赛的通知

经研究，立达设计奖·国际大学生校园设计大赛组委会决定启动2025 年立达设计奖·第四届国际大学生校园设计大赛。欢迎各大高校按照参赛办法及参赛流程参赛。

详见网址：http://chinaccsis.com/Data/View/885

关于举办 2025 年全国大学生商科综合能力大赛——全国总决赛的通知

2025 年全国大学生商科综合能力大赛由中国创造学会主办，中国传媒大学经济与管理学院、上海策鸿信息科技有限公司。根据安排，现决定 2025 年全国大学生商科综合能力大赛全国总决赛以线上方式举行。

详见网址：http://chinaccsis.com/Data/View/888

☆新闻动态☆

中国创造学会与国际艺术设计与媒体院校联盟（CUMULUS）达成合作，开启创新合作新篇章！

2025 年 6 月 5 日，中国创造学会与国际艺术设计与媒体院校联盟（CUMULUS）在法国南特 CUMULUS 2025 年国际会议上正式签订合作备忘录。中国创造学会理事长娄永琪、CUMULUS 主席 Lorenzo Imbesi，秘书长 Eija Salmi 出席并签署相关文件。

详见网址：http://chinaccsis.com/Data/View/881

创造万岁！祝贺中国创造学会成立 31 周年！

中国创造学会（简称“中创会”）经中国科学技术协会、国家科技部、国家民政部批准、发证，于 1994 年 6 月 9 日在上海正式成立。

今天是中创会成立 31 周年纪念日！

向 31 年来为中创会无私奉献的人们致敬！

详见网址：http://chinaccsis.com/Data/View/875

第八届全国大学生创新体验竞赛颁奖典礼圆满举行

2025 年 6 月 2 日，第八届全国大学生创新体验竞赛颁奖典礼暨江宁开发区大学生创业项目签约落户仪式在东南大学国家大学科技园举行。本次竞赛由中国创造学会主办。

详见网址：

https://mp.weixin.qq.com/s/6VK_JkTlvR44x30nbY22BA

第八届中国（上海）国际发明创新展览会圆满完成

2025 年 6 月 11 日-13 日，第十一届中国（上海）国际技术进出口交易会（简称“上交会”）在上海世博展览馆开幕，本届展会由上海发明协会主办，中国创造学会、上海市科技创业中心、上海市科学技术交流中心等单位联合协办。

详见网址：http://chinaccsis.com/Data/View/884

中国创造学会驻京津冀区域协同办事处、中国创造学会人才教育培养专业委员会与雄安新区人才发展集团创新合作交流会成功举办

2025 年 6 月 16 日，中国创造学会驻京津冀区域协同办事处（以下简称“办事处”）、中国创造学会人才教育培养专业委员会（以下简称“专委会”）与雄安新区人才发展集团于廊坊成功举办协同创新合作对接交流会。

详见网址：http://chinaccsis.com/Data/View/882

☆专家声音☆

新质生产力与脑机接口

李德伟

6 月 29 日我国首个脑机接口未来产业集聚区“脑智天地”在上海启动建设。它地处上海新虹桥国际医学中心，将发挥重点区域产业和临床资源优势，推动脑机接口创新资源集聚、技术产业协同发展，培育具有国际影响力的未来产业集群。脑机接口是实现大脑与外部设备信息交互的交叉前沿技术，在医疗、康养、教育、娱乐等领域有广阔的应用前景。今年 1 月《上海市脑机接口未来产业培育行动方案（2025—2030）》发布，进一步加速了产品研发和临床试验。目前上海在侵入式、半侵入式和非侵入式赛道相继涌现出创新成果和创业企业，布局建设了相关重点实验室和公共服务平台，已成为国内覆盖全技术领域的脑机接口创新策源高地。

让盲人恢复视力，用人脑连接 AI。马斯克的脑机接口想要“改变人类”，埃隆·马斯克再次交出了一份“未来式”的答卷。6 月 28 日 Neuralink 公布了 2025 年夏季的阶段性进展，在一场长达一个小时的发布会中展示了已植入设备的志愿者如何仅靠脑信号控制电脑光标、绘图、打游戏，甚至操作 Tesla 旗下 Optimus 机器人手臂的画面。岩思类脑首席科学家、中国科学院上海微系统所研究员李孟解释说，可以将脑机接口系统理解为大脑意念的翻译器，大脑思考时会源源不断地释放脑电波，岩思类脑研发的系统能解码脑电波。“脑电解码性能

的高低，决定了脑机接口系统的智能化水平。我们凭借国内领先的神经编解码技术，能精准读取脑电信号的意图，而且达到 60 毫秒的高刷新率，让玩家戴上非侵入式的脑电帽，就能完成实时、连续的意念操作。”未来这种技术有望广泛应用于医疗康复、教育、游戏娱乐、智能家居、工业控制、航空航天等领域，把大脑变成“遥控器”，为人类增加一个信息交互维度，也为有行动障碍的人带来生活便利。

脑机接口 Brain Computer Interface，是一种直接建立人脑与外部设备之间的沟通通道的技术。其核心理念在于通过读取大脑电信号，将意图转化为指令，进而控制外部设备。这一技术正随着 AI 技术的发展而不断演进。AI 的强大数据处理与学习能力，使得脑机接口在信号解读、用户体验优化以及个性化应用等方面具备了更高的潜力。关键技术与应用场景。信号处理与解码技术：传统的脑机接口依赖于固定的信号模式进行解读，而新一代脑机接口结合深度学习算法，能够实时分析大脑活动，通过训练大规模神经网络，提升解码精度。例如，哈佛大学的研究团队成功开发了基于 AI 的脑机接口，帮助瘫痪患者通过思考来控制假肢。

医疗领域：AI 与脑机接口的结合，为医疗康复提供了新的思路。利用这种技术，医生能够监测病人的大脑活动状态，制定个性化康复计划。2024 年，瑞士一家医疗机构成功实施了一项临床试验，参与者通过脑机接口控制虚拟现实设备进行康复训练，从而显著提升了运动功能。增强人类能力：脑机接口不仅用于治疗疾病，还可以用来增强正常人类的能力。例如，一些企业正在研究如何通过脑机接口实现更快速的信息处理与决策，从而提升职场效率。这种技术的商业化前景，

吸引了众多科技巨头的关注与投资。2023 年 12 月，脑机接口入选“2023 年度十大科技名词”，脑机接口被工信部定义为未来产业。

脑机接口是生物技术与信息技术的跨界融合，是新一轮科技革命和产业革命的重要驱动力，是 BT（生物科技）+IT（信息科技）领域最活跃的研究方向之一，将改变人类与世界的信息交互方式；其将掀起一场数字生命革命，重塑创新链和产业链。脑机接口（BCI）作为人机融合的核心技术，正从实验室走向产业化，深刻重塑医疗、工业及人类认知边界。以下从技术原理、应用场景、产业生态、挑战争议及未来趋势五个维度深度解析：

技术原理：人脑与机器的信号桥梁

1.信号采集层

技术路线	原理	代表设备	性能瓶颈
侵入式	电极植入皮层/脑实质	Neuralink（1024 通道）、脑虎科技（256 通道）	生物相容性、免疫排斥
半侵入式	电极贴敷硬脑膜外	“北脑一号”、Synchron 血管内支架	信号衰减（颅骨阻隔）
非侵入式	头皮贴附 EEG/fNIRS 传感器	博睿康 NEO 头盔、OpenBCI 头环	信噪比低（仅 6-10dB）

2.信号解码层。算法演进：传统模型：LDA、SVM（识别简单运动意图）；深度学习：CNN 处理空间特征（如手势识别准确率 92%）、LSTM 捕捉时间序列（语言解码）；融合创新：清华团队“脑语者”系

统结合 Transformer，汉语解码延迟降至 80ms。3.反馈执行层。双向交互：输出控制：意念操控机械臂/外骨骼（博睿康系统响应延迟<200ms）；输入反馈：Neuralink“Blindsight”向视觉皮层输入电信号，助盲人感知光影。

医疗应用：从功能替代到能力增强

1.神经功能重建

疾病领域	技术方案	临床成效	代表案例
截瘫/渐冻症	侵入式 BCI+机械臂	患者自主喝水、打字交流（62 词/分钟）	中国首例植入患者（2025）
失语症	汉语脑电解码	意念生成句子（准确率 71%）	脑虎科技 256 通道系统
帕金森	闭环深部脑刺激	癫痫发作减少 75%	北京天坛医院临床验证

2.主动康复范式。卒中康复：BCI 外骨骼实时感知运动意图，驱动肌肉电刺激（华西医院“魔笛”系统，功能恢复率达 78%）。认知干预：阿尔茨海默病早期脑电筛查+颅磁刺激，延缓病程进展 3-5 年。

产业生态：中美竞速与国产突围

1.全球格局

国家	技术优势	代表企业	战略布局

美国	高通道侵入式芯片（Neuralink）	Synchron、Blackrock	DARPA 资助军事应用
中国	柔性电极/汉语解码	脑虎科技、阶梯医疗、博睿康	“十四五”脑科学专项
欧盟	非侵入式伦理标准	MindMaze、g.tec	《神经技术伦理法案》

2.国产化突破。芯片：海南大学 SX-R128S4 芯片（128 通道，延迟<5ms，功耗降 80%）；电极：阶梯医疗超柔性电极（直径 1μm，排异反应低于 Neuralink）；系统：“北脑一号”半侵入式设备（三甲医院装机量超 50 台）。

核心挑战：技术-伦理-成本三角困局

1.技术壁垒。信号质量：非侵入式信噪比不足（颅骨衰减 90%信号），侵入式长期稳定性待解（6 个月后电极失效率达 30%）；解码瓶颈：汉语需处理 407 个音节组合，算力需求超英文 3 倍；带宽限制：人脑每秒产生 1TB 数据，现有系统仅能处理 0.001%。

2.伦理争议。隐私黑洞：脑电数据可暴露潜意识（如政治倾向、性取向），欧盟立法禁止未授权解码。认知操纵：哈佛实验通过 BCI 植入虚假记忆，引发“意识主权”争议。社会公平：侵入式设备单套 25 万美元，或加剧阶层分化。

3.产业化障碍。成本困境：256 通道柔性电极量产成本仍超$10 万/套。标准缺失：中国虽发布 24 项团体标准（如 T/GXDSL007-2025），但缺乏强制认证体系。医工割裂：医生与工程师需求错位，导致临床转化周期长达 5-8 年。

未来趋势：脑机智能网络的终极形态

1.技术融合。AI 赋能：LaBraM 大模型提升汉语解码准确率至 90%。量子接口：中科大团队探索量子传感器采集神经信号，抗干扰能力提升百倍。生物杂交：类器官芯片（Brainoware）替代传统电极，实现“人-生物脑-机器”三级交互。

2.场景升维

领域	演进方向	关键技术
医疗	从治疗到增强	记忆植入、情绪调控
工业	脑控人机协作	意念操控工程机械（三一重工试验）
国防	士兵-无人机群脑网协同	DARPA“脑控蜂群”项目
元宇宙	意识直连虚拟世界	Neuralink“心灵感应”接口

3.治理框架。神经权利法案：明确脑数据归属权、禁止强制解码。全球标准联盟：推动 ISO/IEC JTC1 工作组制定 BCI 互操作标准。普惠医疗：医保覆盖 BCI 植入手术（北京试点报销 50%）。

4.终极命题：人类会成为“半机械人”吗？短期（2025-2030）：医疗刚需驱动 BCI 普及，渐冻症/截瘫患者优先获益；中期（2030-2040）：非侵入式设备消费化，意念控制智能家居成为常态；长期（2040+）：脑机融合突破“颅骨枷锁”，人类认知能力指数级增强——生物学人类终结，人机共生文明开启。脑机接口的本质是扩展人类进化边界：当大脑直连云端，知识获取无需学习；当意识操控万物，肢体不再是行动枷锁。然而技术越颠覆，越需警惕“意识殖民”风险——唯有建立全球伦理防火墙，方能确保技术向善。

脑机接口（BCI）作为融合神经科学、人工智能和材料学的颠覆性技术，正通过医疗、工业及人机交互等领域的深度应用，成为新质生产力的核心引擎。以下从技术突破、产业变革和挑战机遇三方面展开分析：

技术突破：医疗与工业场景的效能革命

1.医疗效能跃迁。神经疾病诊疗：天津大学“神工系列”非侵入式 BCI 将脑积水诊断时间从 3 天压缩至 30 分钟，已应用于北京航天总医院等三甲医院；其“神心”系统实现抑郁症诊疗国产化，“神甲”助力脑卒中患者运动功能重建。重症康复创新：上海博睿康、脑虎科技等企业通过侵入式 BCI 使瘫痪患者实现“意念操控”（如自主饮水、控制智能设备），阶梯医疗的长期植入试验让截肢患者用脑电玩赛车游戏。语言功能重建：西湖灵犀科技突破汉语解码技术，将脑电信号转化为完整句子，正确率达 30%，为失语患者提供交流新路径。

2.工业安全升级。华脑技术开发的 BCI 智能安全帽，结合干电极与抗噪算法，实时监测隧道施工人员的疲劳状态，在北京地铁 13 号线等工程中降低事故率 30%以上，推动高风险作业从“被动防护”转向“主动预警”。产业生态：创新集聚与跨界融合。1.全链条协同范式。上海“脑智天地”集聚区整合华山医院临床资源、岩思类脑算法平台及临港集团制造能力，构建“临床需求-技术研发-应用验证”闭环。例如医生与工程师共研植入方案，使反馈周期缩短 50%。2.国产化技术布局，非侵入式：天津大学开发 20 余款“神工”产品，覆盖诊断、治疗全流程。侵入式：中科院刘冰团队研发“脑-机双学习”

系统，通过柔性电极与神经适配算法实现视觉重建与运动控制，填补国内技术空白。

3.资本与政策赋能。上海发布专项培育方案（2025-2030），设立脑机接口产业基金；杭州通过“西湖英才计划”提供场地与资金扶持灵犀科技等企业。

核心挑战：技术瓶颈与伦理风险

1.技术壁垒。信号质量：非侵入式 BCI 信噪比仅 6-10dB，易受颅骨衰减干扰；侵入式虽精度高，但柔性电极的长期生物相容性（如免疫反应）仍未完全解决。解码瓶颈：汉语等复杂语言需处理 407 个音节组合，算法算力要求极高；运动控制中脑电与刺激的匹配精度不足。系统局限：带宽延迟（>8ms）制约实时交互，微型化植入器件（<3mm^3）和功耗（>5mW）待优化。

2.伦理与治理困境。隐私风险：美国政府报告指出 BCI 数据可能被未授权访问，医疗与非医疗场景的隐私保护边界模糊。公平性质疑：侵入式设备单套成本超 25 万美元，可能加剧医疗资源不平等；徐英瑾等学者警示“技能捷径”可能颠覆“努力-回报”的社会伦理基础。

未来路径：新质生产力的重构方向

1.技术融合。结合 CNN/LSTM 提升脑电解码效率，利用联邦学习破解医疗数据隐私难题；发展超声微创植入方案降低手术风险。

2.场景拓展。从医疗康复向多领域延伸：工业：危化品运输司机状态监测；消费电子：意念控制智能家居；国防：脑控机器人协同作业。

3.治理创新。需建立三级伦理审查（如 IEEE P2731 标准）、开源脑电数据集共享机制，并制定专用医保覆盖指南（借鉴美国 GAO 报告建议）。

脑机接口（BCI）技术在医疗领域的应用正从实验室快速走向临床实践，通过神经信号解码与外部设备控制，为传统医学难题提供突破性解决方案。以下是其在医疗场景中的核心应用及最新进展。

运动功能重建：瘫痪患者的“数字桥梁”

1.肢体操控替代。侵入式系统：中国首例侵入式 BCI 临床试验中（2025 年 3 月），四肢截肢患者通过硬币大小的植入体（直径 26mm，厚 6mm）连接超柔性电极（直径≈头发丝 1/100），仅训练 2-3 周即实现意念操控电脑下棋、玩赛车游戏，精度接近正常人触摸板操作水平。机械臂控制：博睿康 NEO 植入系统使瘫痪患者实现自主喝水、下床活动；下一步计划将扩展至机械臂抓取、机器狗操控等复杂物理交互。

2.外骨骼协同。三一重工开发的 BCI 外骨骼系统，提升工人操作精度 60%，降低疲劳度 35%；华西医院“魔笛”系统识别运动意图仅需 300 毫秒，驱动外骨骼辅助卒中患者行走。

神经疾病诊疗：精准干预的新范式

1.癫痫与帕金森病管理。闭环神经刺激：创新医疗的闭环 BCI 系统将癫痫发作频率降低 75%，相关设备已纳入北京医保。早期预警：基于 α－β 波段 EEG 特征的帕金森病预警模型（AUC=0.89），结合深度学习实时监测异常神经信号。

2.精神疾病干预。抑郁症治疗：脑电生物反馈技术使治疗有效率提升至 68%（传统疗法 46%），通过调节前额叶皮层活动改善情绪。阿尔茨海默病筛查：非侵入式 BCI 捕捉轻度认知障碍脑电特征，结合颅电磁刺激形成“早筛-干预”闭环。

手术与康复：临床痛点的技术破局

1.脑肿瘤精准切除。华西医院在脑胶质瘤手术中应用 8×8 电极侵入式 BCI，实时区分肿瘤与正常脑组织边界，将致残率从 70%降至 10%以下，降低基层医生操作门槛。

2.卒中主动康复。“魔笛”系统：患者佩戴类头盔设备，BCI 识别运动意图后触发电刺激肌肉，重建神经通路，实现社区/家庭康复。疗效提升：BCI 驱动的康复训练使脑卒中患者运动功能重建成功率提升至 78%，专注力训练覆盖 3200 所学校，学生专注力提升 43%。

语言与感官功能重建：打破沉默与黑暗

1.失语症沟通。脑虎科技 256 通道柔性 BCI 实现汉语实时解码（准确率 71%），渐冻症患者通过意念发送文字消息；西湖灵犀科技

汉语解码正确率达 30%，为全球最大失语群体（5000 万）提供表达可能。

2.视觉恢复探索。Neuralink“Blindsight”技术刺激猴子视觉皮层识别虚拟物体（准确率 66%），目标为盲人恢复基础视力并扩展至红外感知等“超人视觉”。

挑战与未来方向

1.技术瓶颈。信号质量：非侵入式信噪比仅 6-10dB，侵入式电极长期生物相容性待提升（如免疫反应）。成本限制：侵入式系统单套超 25 万美元，普惠化需医保覆盖与国产替代（如海南大学芯片降本至 30 万元内）。

2.伦理与标准化。隐私风险：神经数据需联邦学习等隐私计算技术保护，禁止跨场景滥用。临床规范：中国正加速制定标准（如《非侵入式设备通用技术条件》），建立三级伦理审查机制。

3.未来演进。短期（2025-2027）：聚焦运动/语言重建产品落地，推动医保覆盖。长期（2030+）：结合 AI 大模型（如 LaBraM）实现记忆增强、情绪调控，迈向“人机共生”。

脑机接口（BCI）作为新质生产力的核心引擎，其技术突破与产业落地高度依赖标准化建设。当前全球竞争格局下，中国正通过政策引导、技术规范与产业协同加速构建 BCI 标准体系，以解决技术异构性、伦理风险及产业化瓶颈。以下是关键进展与挑战的深度分析。

政策驱动：国家级标准体系加速构建

1.顶层设计与地方行动。北京方案：明确将“标准创制”列为五大重点任务，要求建立核心指标检测评价方法，推动技术、数据、伦理等维度的标准制定，缩短产品研发周期。上海行动：依托“脑智天地”集聚区，建立脑机接口临床试验与转化重点实验室，推动产学研医共建创新联合体，实现“临床需求-技术研发-应用验证”闭环。四川计划：提出到2030年完成侵入式手术3000例/年，同步配套医疗服务价格（如侵入式置入费6552元/次），为商业化铺路。

2.团体标准先行。成都锦城学院专家工作站牵头制定24项国家级团体标准，覆盖BCI全链条。硬件层：如《植入式脑机接口设备设计与制造规范》（T/GXDSL007—2025）；数据层：如《脑机接口数据采集与存储规范》（T/GXDSL008—2025）；应用层：如《脑机接口在智能家居控制中的应用规范》（T/GXDSL011—2025）。

技术标准框架：从医疗到多场景覆盖

1.医疗领域优先突破。非侵入式设备国标：2025年6月，《非侵入式设备通用技术条件》国家标准公开征求意见，首次统一信号采集质量、解码准确率、穿戴力学性能等测试方法。临床规范：团体标准细化至病症场景，如《脑机接口老年痴呆疾病临床应用规范》（T/GXDSL049—2024）和《脑机接口AI手功能康复系统技术规范》（T/GXDSL050—2024）。

2.跨领域兼容性标准。工业安全：要求BCI设备在强电磁干扰环境下稳定运行，如隧道施工人员疲劳监测系统需通过抗噪算法认证。

消费电子：制定《脑机接口脑电信号采集技术规范》（T/GXDSL006—2025），确保智能家居脑控设备的低延迟（<8ms）与高泛化性。

3.核心性能指标统一

技术维度	标准要求	测试方法
信号采集信噪比	非侵入式≥6dB，侵入式≥20dB	模拟颅骨衰减环境测试
解码延迟	医疗场景≤10ms，工业场景≤15ms	实时运动控制反馈实验
穿戴舒适性	连续佩戴 8 小时皮肤压痕深度≤0.5mm	力学传感器多点监测
系统功耗	植入式设备≤5mW，无线传输≤2mW	恒温加速老化试验

产业协同：以标准打通创新链-产业链

1.平台化赋能。北京：建设脑机接口大数据公共服务平台，推动数据脱敏共享；设立概念验证中心加速工程化转化。上海“脑智天地”：集成华山医院临床资源、岩思类脑算法平台及临港制造能力，使技术反馈周期缩短 50%。

2.企业梯度培育。领军企业：如脑虎科技（256 导柔性 BCI）、博睿康（NEO 植入系统）主导高精度标准制定；中小企业：汉威科技量产柔性电极降低成本 50%，推动硬件标准化。

伦理与安全标准：技术落地的“刹车系统”

1.隐私与数据安全。要求 BCI 数据存储需符合《计算中心数据隐私保护标准》（T/GXDSL020—2025），采用联邦学习技术实现分布式

训练。禁止未授权脑电数据跨场景使用（如医疗数据用于消费行为分析）。

2.伦理审查机制。建立三级审查体系：机构伦理委员会→区域审查中心→国家科技伦理委员会，参考 IEEE P2731 标准。植入式设备需通过长期生物相容性测试（如阶梯医疗 6 个月免疫反应追踪）。

挑战与未来路径

1.待解难题。技术异构性：侵入式与非侵入式设备性能差异大，需分路径制定标准；国际互认滞后：仅 23%中国标准与国际接轨，影响产品出海；成本公平性：侵入式设备单套成本超 25 万美元，需医保覆盖指南（借鉴美国 GAO 报告）。

2.标准化 2.0 方向。动态迭代：每 2 年更新算法效能基准（如汉语解码正确率从 30%提至 50%）；跨技术融合：联合 AI 大模型（如 LaBraM）、量子通信标准，构建“BCI+”复合标准群；全球协作**：推动中国主导的 ISO/IEC JTC1 脑机接口工作组，输出“上海方案”。

脑机接口如何定义新质生产力？

脑机接口正从三方面重塑生产力范式。效率革命：医疗诊断效率提升百倍，工业事故率显著下降；认知拓展：突破生理限制，重建运动/语言/视觉功能；产业重构：带动“材料-算法-临床-制造”千亿级产业链。其发展需攻克“信号-算法-伦理”三角瓶颈，最终实现从“替代功能缺失”到“增强人类能力”的质变，成为新质生产力的核

心支点。医疗范式的重塑。脑机接口已从“功能替代”迈向“能力增强”阶段。功能修复：重建运动、语言、视觉，解决截瘫、失语等顽疾；诊疗革新：癫痫/抑郁精准干预、脑癌手术降风险；康复普惠：居家主动训练，降低医疗负担。随着国产超柔性电极、汉语解码等关键技术突破，以及上海“脑智天地”等产业生态构建，BCI 正成为新质生产力在医疗领域的核心引擎，但其规模化仍需攻克“技术-成本-伦理”三角难题。

脑机接口技术涉及硬件、软件、信号解码、能源管理等多个复杂环节，每一项都需要突破技术瓶颈。脑机接口与机器人的融合正催生万亿级新业态，医疗康复领域已进入商业化爆发前夜。脑机接口关键设备的国产替代是中国突破技术封锁、抢占产业高地的核心战略，已在芯片、电极、系统集成等环节实现重大突破。如技术验证明确（如爱朋医疗、岩山科技）、产业链整合能力强（如汉威科技、南京熊猫）的标的，长期需跟踪技术迭代速度与临床转化效率，把握人机交互革命带来的结构性机会。国产替代不仅是技术替代，更是标准与生态的重新定义。中国在柔性电极、汉语解码等局部领域已实现“并跑”，下一步需通过临床需求反哺技术迭代、政策资本双轮驱动，在“人机共生”的终极竞争中掌握话语权。

标准定义脑机接口的未来。短期（2025-2027）：医疗设备标准驱动临床转化，非侵入式产品规模化商用；中期（2028-2030）：工业、消费电子多场景标准成熟，成本下降催生千亿市场；长期（2030+）：脑机融合智能标准突破认知边界，伦理框架全球趋同。标准化建设正从“跟随式规范”转向“引领式创新”，成为 BCI 从实

验室奇观迈向新质生产力的核心枢纽。唯有攻克“技术-伦理-产业”三角标准化的协同难题，方能在人机共生的未来竞争中掌握定义权。

作者简介：李德伟 中国创造学会创研委副主任
中国贸促会商业行业委员会上海标准化服务中心主任
上海中小企业国际合作协会特聘副会长
上海市浦东新区管理咨询行业协会专精特新服务专业委员会主任
著作《创新缔造竞争力》等

☆专家声音☆

发展新质生产力：以创新赋能乡村振兴——上海市公共数据授权运营的实践探索与策略建议

徐晓光

摘要

在数字化转型的浪潮中，公共数据作为新型生产要素，其创新应用对于推动乡村振兴具有不可估量的价值。本文以上海市为例，探讨公共数据授权运营在乡村振兴领域的实践探索，分析存在的问题，并提出融合创新理念的策略建议，以期为全国数字乡村建设提供新思路。

关键词：公共数据授权运营；乡村振兴；创新赋能；数据治理

一、引言

随着信息技术的飞速发展，数据已成为推动社会经济发展的重要资源。公共数据，作为政府及公共机构在履行职责过程中产生或获取的数据资源，其开放共享与授权运营对于促进数字经济发展、提升社会治理能力具有重要意义。特别是在乡村振兴战略背景下，如何创新公共数据应用模式，赋能乡村产业发展、提升乡村治理水平，成为亟待探索的重要课题。

中国创造学会作为致力于推动创新理论与实践研究的学术团体，始终关注数据要素在创新驱动发展战略中的作用。本文旨在从创新视

角出发，分析上海市公共数据授权运营在乡村振兴领域的实践案例，揭示存在的问题，并提出具有创新性的策略建议。

二、上海市公共数据授权运营赋能乡村振兴的创新实践

上海市作为全国改革开放的前沿阵地，在公共数据授权运营方面进行了积极探索，形成了一系列创新实践，为乡村振兴注入了新动能。

数据驱动的乡村产业创新：

案例一：浦东新区“神农口袋”APP：该应用通过整合农业、气象、土地等多源数据，为农户提供精准种植建议、市场行情分析等服务，实现了农业生产过程的数字化管理。其创新点在于构建了“数据+服务”的新模式，将原本分散的数据资源转化为直接服务于农业生产的生产力。

案例二：奉贤区农业要素交易所：通过搭建线上线下融合的交易平台，促进农业资源的高效配置。其创新之处在于利用公共数据打破信息不对称，推动农业产业链上下游的深度融合，激发了乡村产业活力。

数智融合的乡村治理创新：

案例三：松江区新浜镇数智乡村振兴计划：该计划通过 5G 网络覆盖、无人农场、智慧安防等应用，实现了乡村治理的智能化升级。其创新点在于将先进信息技术与乡村治理深度融合，提升了治理效能和村民获得感。

机制创新的受益分配模式：

案例四：光明食品集团数据资产化探索：作为国企，光明食品集团积极参与公共数据授权运营，通过数据清洗、分析、建模等环节，将农业数据转化为具有经济价值的数据产品。其创新之处在于探索数据资产化的新路径，为数据收益分配提供了新思路。

三、存在的问题与创新挑战

尽管上海市在公共数据授权运营赋能乡村振兴方面取得了显著成效，但仍面临一些问题和挑战，需要以创新思维寻求破解之道。

数据质量与标准化难题：

问题表现：数据来源广泛、采集标准不一，导致数据质量参差不齐，标准化程度不足。

创新挑战：如何运用区块链、人工智能等新技术，建立数据质量智能评估与动态优化机制，提升数据标准化水平？

受益分配机制不完善：

问题表现：数源部门、运营机构、开发主体等各方利益分配机制尚不健全，农户受益不明显。

创新挑战：如何设计基于数据贡献度的动态收益分配模型，构建农户直接受益机制，激发各方参与热情？

技术壁垒与安全风险：

问题表现：农村地区信息技术基础设施薄弱，专业人才匮乏，数据安全风险突出。

创新挑战：如何研发适用于乡村场景的轻量化、低成本信息技术解决方案，构建数据安全防护体系？

数据共享与协同障碍：

问题表现：部门间数据共享不足，跨区域数据协同困难。

创新挑战：如何建立跨部门、跨区域的数据共享激励机制，打破数据孤岛，实现数据资源的互联互通？

四、融合创新理念的策略建议

针对上述问题与挑战，本文提出以下融合创新理念的策略建议，以期推动上海市公共数据授权运营赋能乡村振兴迈向新台阶。

构建数据治理创新体系：

建议一：建立数据质量智能评估与动态优化机制：运用区块链技术确保数据溯源可信，利用人工智能算法对数据进行自动清洗、校验和标准化处理，提升数据质量。

建议二：推进数据标准化建设与创新应用：加快制定乡村振兴领域关键指标的标准化编码规则，推动跨部门数据融合和共享。同时，鼓励企业、高校、科研机构等参与数据标准制定，形成开放共治的数据治理格局。

优化受益分配创新机制：

建议三：设计基于数据贡献度的动态收益分配模型：根据数源部门、运营机构、开发主体等各方的数据贡献度，运用博弈论、多目标优化等方法，设计科学合理的收益分配比例。同时，探索建立农户数据资产账户，实现数据收益的直接分配。

建议四：构建农户直接受益的创新机制：通过数据资产凭证、数据分红等方式，让农户直接分享公共数据授权运营带来的收益。同时，加强对农户的数据素养培训，提升其利用数据进行创新应用的能力。

突破技术壁垒与加强安全保障：

建议五：研发适用于乡村场景的轻量化信息技术解决方案：针对农村地区信息技术基础设施薄弱的问题，研发低成本、易部署的物联网设备、云计算平台等，降低技术门槛。

建议六：构建数据安全防护创新体系：综合运用加密传输、访问控制、数据脱敏等技术手段，确保数据安全。同时，建立数据安全应急响应机制，提升安全风险防范能力。

促进数据共享与协同创新：

建议七：建立跨部门、跨区域的数据共享激励机制：通过财政补贴、税收优惠等政策措施，激励部门间、区域间数据共享。同时，建立数据共享绩效评估体系，对共享成效显著的单位和个人给予表彰奖励。

建议八：推动数据资源互联互通与协同创新：加强跨区域数据协同合作，推动建立区域性的公共数据共享平台。通过制定统一的数据

标准和利益分配机制，促进跨区域数据资源的整合和共享。同时，鼓励企业、高校、科研机构等参与跨区域数据协同创新项目，共同推动乡村振兴领域的创新发展。

五、结语

公共数据作为新型生产要素，在乡村振兴中具有巨大的潜力和价值。然而，要实现公共数据授权运营赋能乡村振兴的目标，必须坚持以创新为引领，不断破解数据质量、受益分配、技术壁垒、数据共享等难题。本文提出的策略建议，旨在融合创新理念，为上海市乃至全国的数字乡村建设提供新思路、新路径。我们期待与各界同仁携手共进，以创新赋能乡村振兴，共同绘就数字中国的新篇章。

作者简介：徐晓光 中国创造学会创研委委员
科技部-中国科技咨询协会创业导师工委会副秘书长
致公党上海闵行科技支委委员
共青团中国青年创业就业基金会中央中国青年创业导师
山东省教育厅特聘产教融合专家

☆专家声音☆

Botulinum toxin A prevents hypertrophic scarring by suppressing PARP14/ SOCS2-mediated M2 polarization of macrophages

Mohyeddin Ali[a,1], Bochao Xie[b,1], Pengfei Li[a], Shuwei Chen[a], Yao Lu[a], Fazhi Qia[a,*], Ze Xiong[c,d,e,**], Jianrui Li[a,***]

BBA - Molecular Cell Research 1872 (2025) 120003

Contents lists available at ScienceDirect

BBA - Molecular Cell Research

journal homepage: www.elsevier.com/locate/bbamcr

Botulinum toxin A prevents hypertrophic scarring by suppressing PARP14/SOCS2-mediated M2 polarization of macrophages

Mohyeddin Ali [a,1], Bochao Xie [b,1], Pengfei Li [a], Shuwei Chen [a], Yao Lu [a], Fazhi Qi [a,*], Ze Xiong [c,d,e,**], Jianrui Li [a,***]

[a] Department of Plastic Surgery, Zhongshan Hospital, Fudan University, Shanghai 200032, PR China
[b] Hebei Academy of Chinese Medical Sciences, Shijiazhuang 050000, Hebei, PR China
[c] Wireless and Smart Bioelectronics Lab, School of Biomedical Engineering, ShanghaiTech University, Shanghai 201210, PR China
[d] State Key Laboratory of Advanced Medical Materials and Devices, ShanghaiTech University, Shanghai 201210, PR China
[e] Shanghai Clinical Research and Trial Center, Shanghai 201204, PR China

ARTICLE INFO

Keywords:
Botulinum toxin A
Hypertrophic scars
Macrophages
PARP14
SOCS2

ABSTRACT

Botulinum toxin A (BTXA) is a safe and widely used neurotoxic protein in cosmetic procedures and medical applications. This investigation focuses on the function of BTXA on macrophage phenotype during hypertrophic scar (HS) formation and the underlying functional mechanism. A mouse model of HS was generated, where BTXA treatment reduced dermal thickness, epidermal hyperplasia, and collagen deposition in a dose-dependent manner. Moreover, BTXA reduced fibrosis, proliferation, angiogenesis, and M2 macrophage markers within the scar tissues, with parallel findings obtained in the *in vitro* co-culture system of induced M2 macrophages (derived from THP-1 monocytes) and human dermal fibroblasts (HDFs). Following bioinformatics and RNA sequencing insights, we identified increased expression of poly (ADP-ribose) polymerase family member 14 (PARP14) and suppressor of cytokine signaling 2 (SOCS2) in wound skin of mice, which were suppressed by BTXA treatment. PARP14 enhanced SOCS2 mRNA stability. Overexpression of PARP14 restored the M2 polarization of macrophages and negated the HS-ameliorating effects of BTXA. However, these effects were counteracted by the additional silencing of SOCS2 in mice or THP-1 cells. In conclusion, this investigation suggests that BTXA inhibits PARP14-mediated SOCS2 RNA stabilization to reduce M2 polarization of macrophages and alleviate hypertrophic scarring.

1. Introduction

Hypertrophic scars (HS) frequently emerge following significant skin injuries, such as those caused by trauma, burns, or surgical procedures [21]. HS typically presents as pruritic, painful, elevated, erythematous, and dyschromic, with contractile properties [11]. These symptoms, along with physical deformities such as bulging, redness, and skin tightening, significantly impair the quality of life, physical well-being, and psychological health of affected individuals [5,15]. Although numerous treatment options, including surgical removal, silicone-based treatments, interferons, corticosteroids, laser therapy, pressure therapy, and other anti-collagen therapies, have been proposed for managing HT, an ideal treatment approach remains elusive [8].

The onset and progression of HS are intricately linked to the wound healing process, which is typically divided into several continuous phases: hemostasis, inflammation, proliferation, and remodeling of the extracellular matrix [20,32]. Macrophages are involved in all stages of HS genesis through phenotypic changes [26]. Pro-inflammatory mediators like interferon-γ and tumor necrosis factor induce the formation of "classically activated" M1 macrophages, which produce pro-inflammatory cytokines and support the early stages of wound healing [7]. Conversely, M2 macrophages, activated by interleukin (IL)-4 and/

* Corresponding author.
** Correspondence to: Z. Xiong, Wireless and Smart Bioelectronics Lab, School of Biomedical Engineering, ShanghaiTech University, Shanghai 201210, PR China.
*** Correspondence to: J. Li, Department of Plastic Surgery, Zhongshan Hospital, Fudan University, No. 180, Fenglin Road, Xuhui District, Shanghai 200032, PR China.
E-mail addresses: dr_qifazhi@126.com (F. Qi), xiongze@shanghaitech.edu.cn (Z. Xiong), leejianrui@163.com (J. Li).
[1] These authors contributed equally to this work

https://doi.org/10.1016/j.bbamcr.2025.120003
Received 10 February 2025; Received in revised form 3 June 2025; Accepted 8 June 2025
Available online 10 June 2025

or IL-13, secrete anti-inflammatory factors such as transforming growth factor β (TGF-β) and IL-10, promoting fibrosis, angiogenesis, and tissue repair [7]. However, an overabundance of M2 macrophages or delayed M2 cytokine expression is associated with pathological scar formation [31], making them potential therapeutic targets for reducing hypertrophic scarring.

Botulinum toxin (BTX), also referred to as BoNT, is a neurotoxic protein produced by the bacterium *Clostridium botulinum* and related species [1]. It is widely recognized for its applications in cosmetic and medical procedures [9]. Type A BTX (BTXA) is the most commonly used subtype, with proven safety and effectiveness in reducing wound edge tension and improving scar quality [16]. Emerging studies have underscored BTXA's potential in treating HS [2,18]. However, its effects on macrophage phenotype and the underlying mechanisms remain unclear.

This study employed bioinformatics analyses to identify poly (ADP-ribose) polymerase family member 14 (PARP14) and suppressor of cytokine signaling 2 (SOCS2) as genes that are aberrantly expressed in HS and may be downstream targets modulated by BTXA. An intact PARP14 (also named ARTD8 or BAL2) is constructed by macro1, macro2, macro3, WWE, and the catalytic domain, and PARP14 has been considered a fascinating target for the treatment of allergic inflammation since it uses nicotinamide adenine dinucleotide as a metabolic substrate to conduct mono-ADP-ribosylation modification on target proteins, taking part in cellular responses and signaling pathways in the immune system [23]. Additionally, PARP14 has been reported to function as an RNA-binding protein (RBP) that influences RNA stability [29]. SOCS2, a member of the SOCS family, is crucial in negatively regulating cytokine signaling pathways and maintaining immune functions [12]. Notably, SOCS2 has been found to activate the Wnt/β-catenin by regulating the nuclear translocation of β-catenin [34], and activation of β-catenin signaling promotes M2 polarization in macrophages [36]. Based on these findings, this study aimed to explore the role of BTXA in macrophage phenotype and HS development, focusing on the potential involvement of the PARP14/SOCS2/β-catenin axis.

2. Materials and methods

2.1. Animal modeling and treatment

Male C57BL/6 mice (8 weeks old, 19–23 g) were purchased from Vital River Laboratory Animal Technology Co., Ltd. (Beijing, China). All animal procedures were approved by the Animal Ethics Committee of Zhongshan Hospital, Fudan University, and were conducted following the Guide for the Care and Use of Laboratory Animals (NIH, Bethesda, MD, USA). The mice were housed under a 12-h light/dark cycle with free access to food and water. After one week of acclimation, the animals were randomly divided into 7 groups: HS + NS (normal saline), HS + BTXA, HS + TA (triamcinolone acetonide), HS + BTXA + oe-NC (overexpression-negative control), HS + BTXA + oe-PARP14, HS + BTXA + oe-PARP14 + sh (short hairpin RNA)-NC, and HS + BTXA + oe-PARP14 + sh-SOCS2 groups, with the HS + BTXA group further subdivided into low, medium, and high-dose groups of 5 mice each. Each group/subgroup contained 5 mice.

All mice were anesthetized *via* intraperitoneal injection of 0.4 mL/kg fluanisone and 5 mg/kg diazepam. The dorsal hair of the mice was shaved and cleaned. A model of HS was induced by suture-anchored tension in excisional wounds in mice. Briefly, a circular, fully laminated wound with a diameter of 8 mm was created on the back, and concentric plastic fixtures were placed on the wound for immobilization. The hollow inner circle was 8.5 mm in diameter, and the circumference was a cylinder 6 mm high, with the inner circle aligned with the wound. The outer diameter was 16.4 mm and flat. The skin around the outer circumference was secured to the inner cylinder with 6–0 nylon thread so that the trauma was pulled under tension. After modeling, the mice were immediately treated with the respective drugs. In the HS + NS group, mice were injected with normal saline as a control, while the other groups were injected intradermally with 0.5 U, 1 U, and 2 U of BTXA (YK2147, Hubei Yongkuo Technology Co., Ltd., Tianmen, Hubei, China) at five different sites along the wound edge [17] or 0.05 mL/g TA (HY-B0636, MedChemExpress, Monmouth Junction, NJ, USA) [3].

Lentiviruses packaged with oe-PARP14, sh-SOCS2, and their NCs (oe-NC, sh-NC) were applied to the mice's wounds to infect the scar tissue. Five loci were selected at the wound edges, and each mouse received 5×10^{10} TU of lentivirus (10^{12} TU/mL, Shanghai GenePharma Co., Ltd., Shanghai, China). Euthanasia was performed by intraperitoneal injection of sodium pentobarbital (150 mg/kg) at week 2 of the incision, and the scar tissue was harvested for subsequent experiments.

2.2. Isolation of macrophages from mouse scar tissues

Referring to a previous report [25], macrophages were isolated from mouse scar tissues. The tissues were cut into 2–3 mm^2 pieces and incubated with dispase buffer containing 1 mg/mL Dispase II (40104ES80, Yeasen, Shanghai, China), 10 mg/mL G418 (60220ES08, Yeasen), and 3 % fetal bovine serum (FBS, 40131ES76, Yeasen) at 4 °C overnight. This was followed by incubation for 2 h at 37 °C through a collagenase digestion buffer containing 1 mg/mL Collagenase I (40507ES60, Yeasen), 5 mg/mL G418, and 75 U/mL DNase I (10325ES90, Yeasen). The suspension was centrifuged at 4 °C to precipitate the cells, and dead cells were removed by LIVE/DEAD Fixable Blue Dead Cell Stain Kit (L23105, Thermo Fisher Scientific Inc., Waltham, MA, USA). The cells were incubated with BeyoFC Fc Receptor Blocking Solution (Anti-mouse CD16/CD32, C1755M, Beyotime, Shanghai, China) for 5 min and with BeyoFC FITC anti-mouse F4/80 Antibody (AC1175, Beyotime), BeyoFC PE-Cy5 anti-mouse CD45 Antibody (AC1020, Beyotime) for 30 min (both on ice in the dark). Macrophages positive for both CD45 and F4/80 were isolated by flow cytometry for subsequent experiments.

2.3. RNA-sequencing (RNA-seq) analysis

Total RNA was extracted from macrophages in scar tissue from HS + NS and HS + BTXA groups of mice (4 samples each) using the RNeasy mini kit (74,106, Qiagen Company, Hilden, Germany), and the purified RNA samples were quantified using a Nanodrop spectrophotometer. cDNA libraries were prepared from RNA samples using the low-throughput sample protocol of the TruSeq RNA Sample Preparation Kit v2 (15,027,387, Illumina, Inc., San Diego, CA, USA). Briefly, mRNA was purified from total RNA using Ampure magnetic beads with attached poly-T oligonucleotides. The purified mRNA was fragmented using divalent cations and high temperatures. Fragmented mRNA was mixed with random primers and reverse transcriptase and amplified by one polymerase chain reaction (PCR) cycle to generate first-strand cDNA. The first-strand cDNA fragments were then incubated with DNA polymerase I at 16 °C for 1 h to synthesize second-strand cDNA. The resulting double-stranded cDNA fragments were end-repaired and ligated to adapters. The final cDNA libraries were purified and amplified by PCR. The quality and concentration of the cDNA libraries were checked using a Bioanalyzer and DNA 1000 kit (5067–1504, Agilent Technologies, Palo Alto, CA, USA) following the manufacturer's protocol. The libraries were sequenced on an Illumina sequencer. Raw reads from paired-end libraries were provided to QFAB in Fastq files for quality control, mapping, and differential expression analysis. Quality checks of raw read counts from sequencing libraries were performed using the FastQC tool. Differentially expressed genes were calculated using the R software package DESeq2 (v.1.40.0), where ADJUST p value <0.05, $|\mathrm{Log_2FoldChange}| > 1$ was considered significant.

2.4. Histological staining

Mouse scar tissue was fixed in 4 % formaldehyde, dehydrated,

Table 1
Primer sequences for qPCR analysis.

Gene	Forward Sequence (5′-3′)	Reverse Sequence (5′-3′)
CD163 (human)	CCAGAAGGAACTTGTAGCCACAG	CAGGCACCAAGCGTTTTGAGCT
Arg-1 (human)	TCATCTGGGTGGATGCTCACAC	GAGAATCCTGGCACATCGGGAA
Arg-1 (mouse)	CATTGGCTTGCGAGACGTAGAC	GCTGAAGGTCTCTTCCATCACC
PARP14 (human)	GACTGTCGCTATGTGCTTCACG	GGACAAGCTCTCAGTGATCTCC
PARP14 (mouse)	GGTCTCTGTTGATGTGGGCACA	TTCTCGGTGGTCTTCAGGCAGT
SOCS2 (human)	GGTCGGCGGAGGAGCCATCC	GAAAGTTCCTTCTGGTGCCTCTT
TGF-β (mouse)	TGATACGCCTGAGTGGCTGTCT	CACAAGAGCAGTGAGCGCTGAA
GAPDH (human)	GTCTCCTCTGACTTCAACAGCG	ACCACCCTGTTGCTGTAGCCAA
GAPDH (mouse)	CATCACTGCCACCCAGAAGACTG	ATGCCAGTGAGCTTCCCGTTCAG

Note: qPCR, quantitative polymerase chain reaction; Arg-1, arginase 1; PARP14, poly (ADP-ribose) polymerase family member 14; SOCS2, suppressor of cytokine signaling 2; TGF-β, transforming growth factor β; GAPDH, glyceraldehyde-3-phosphate dehydrogenase.

embedded, and sectioned into 3 μm slices. The sections were then deparaffinized with xylene and rehydrated in graded ethanol. For Hematoxylin and eosin (HE) staining, the sections were immersed in hematoxylin solution (C0105M, Beyotime) at room temperature for 5 min, followed by soaking in eosin solution for 2 min. Collagen deposition and fibrosis in the tissue section were examined using Masson's trichrome staining kit (0189S, Beyotime). After staining, the tissue sections were dehydrated, cleared with xylene, and mounted with neutral gum for microscopic observation. The scar cross-sectional area from HE staining and the percentage of fibrotic area in Masson's trichrome staining were evaluated using Image J software.

2.5. Immunohistochemistry (IHC)

Following deparaffinization and rehydration, the scar tissue sections were soaked in antigen retrieval solution at 95 °C for 20 min. Endogenous peroxidase activity was blocked with 3 % hydrogen peroxide, and non-specific binding was blocked with 5 % goat serum for 1 h. The sections were then incubated at 25 °C for 1 h with antibodies against CD31 (1:2000, ab182981, Abcam Inc., Cambridge, MA, USA), Ki67 (1:1000, ab15580, Abcam), and CD163 (1:500, ab182422, Abcam). The sections were then incubated at 25 °C with HRP-conjugated goat anti-rabbit IgG (1:30,000, ab205718, Abcam) for 15 min. After visualization using 3,3′-diaminobenzidine (P0202, Beyotime), the sections were washed with phosphate-buffered saline (PBS), counterstained with hematoxylin, and dehydrated for observation under the microscope. The positive staining rate was calculated.

2.6. Cell culture and treatment

The human monocytic cell line THP-1 (CL-0233) was purchased from Procell Life Science & Technology Co., Ltd. (Wuhan, Hubei, China). THP-1 cells were cultured in RPMI-1640 (11,875,093, Thermo Fisher) supplemented with 10 % FBS and 100 U/mL penicillin-streptomycin at 37 °C with 5 % CO_2. THP-1 cells were stimulated with 320 nmol/L phorbol 12-myristate 13-acetate (PMA) (CS0001, Multi Sciences (Lianke) Biotech Co., Ltd., Hangzhou, Zhejiang, China) for 18 h to differentiate into M0 macrophages.

To induce an M2 phenotype, the THP-1 cells were treated with 320 nmol/L PMA for 12 h, followed by further incubation with 20 ng/mL IL-4 (200–04, Peprotech Inc., Rocky Hill, NJ, USA) and 20 ng/mL IL-13 (200–13, Peprotech) for 48 h [30]. For drug treatment, cells were incubated with 30 U/mL BTXA in the presence of IL-4/IL-13 treatment for 24 h. Control cells were treated with an equivalent volume of PBS.

For gene interventions, before PMA treatment, THP-1 cells were infected with oe-PARP14, sh-SOCS2, or NC lentiviruses (MOI = 10) in the presence of 4 μg/mL polybrene (S2667, Sigma-Aldrich, Merck KGaA, Darmstadt, Germany). After 48 h, stably transfected cells were selected with 1.5 μg/mL puromycin for 5 d.

2.7. Cell co-culture assays

Human dermal fibroblasts (HDFs, CL0277, Fenghui Biotechnologies, Changsha, Hunan, China) were seeded in a 75 cm^2 culture dish with DMEM (11,965,092, Thermo Fisher) containing 10 % FBS at 37 °C with 5 % CO_2. A six-well Transwell chamber (0.4 μm, 3412, Corning Glass Works, Corning, NY, USA) was used to develop the co-culture system. HDFs were seeded in the apical chambers at a density of 1×10^4 cells/cm^2. The induced M2 macrophages were seeded at the same density in the basolateral chambers. The co-culture system was maintained for 48 h. After co-culture, cells were harvested for subsequent experiments.

2.8. Enzyme-linked immunosorbent assay (ELISA)

The levels of TGF-β in the supernatant of the differentially treated THP-1 cells (macrophages) were determined using the specific ELISA kit (88–8350-88, Thermo Fisher Scientific). The supernatant was centrifuged at 300 ×*g* for 10 min, and aliquots of the supernatant were collected and stored at −20 °C to avoid repeated freeze-thaw cycles. The measurement was performed using the microplate reader, with the wavelength set to 450 nm.

2.9. Reverse transcription-quantitative polymerase chain reaction (RT-qPCR)

Total RNA was extracted from THP-1 cells and mouse scar tissue using TRIzol reagent (15596026CN, Thermo Fisher Scientific). Total RNA was subjected to agarose gel electrophoresis (Fig. S1A). Only three single bands, 28S RNA, 18S RNA, and 5S RNA, were present. The ratio of the brightness of the 28S to the 18S bands was roughly 2:1, while the 5S RNA bands were so faint that they were hardly observed, indicating that the extracted RNA was of good integrity and high quality. The RNA was reverse-transcribed into cDNA using the RevertAid Reverse Transcription Kit (K1691, Thermo Fisher Scientific). PCR amplification of the internal reference GAPDH was performed, and the quality of cDNA was detected by agarose gel electrophoresis (Fig. S1B). Clear, bright GAPDH band signals were observed, indicating good quality of cDNA. To quantify mRNA expression, fluorescence quantitative PCR (qPCR) analysis was performed using PowerUp SYBR Green Master Mix (A25742, Thermo Fisher Scientific) and cDNA template. With GAPDH serving as the reference gene, the relative expression of target mRNA was calculated using the $2^{-\Delta\Delta Ct}$ method. The primer sequences are shown in Table 1.

2.10. Western blot (WB) analysis

THP-1 cells, HDFs, and mouse scar tissue were lysed in RIPA buffer (89,901, Thermo Fisher Scientific) to extract proteins from whole cell fractions. In addition, nuclear fractions from THP-1 cells and macrophages isolated from scar tissue were extracted by the Nucleus Protein Extraction Kit (EX1470, Solarbio, Beijing, China). The protein

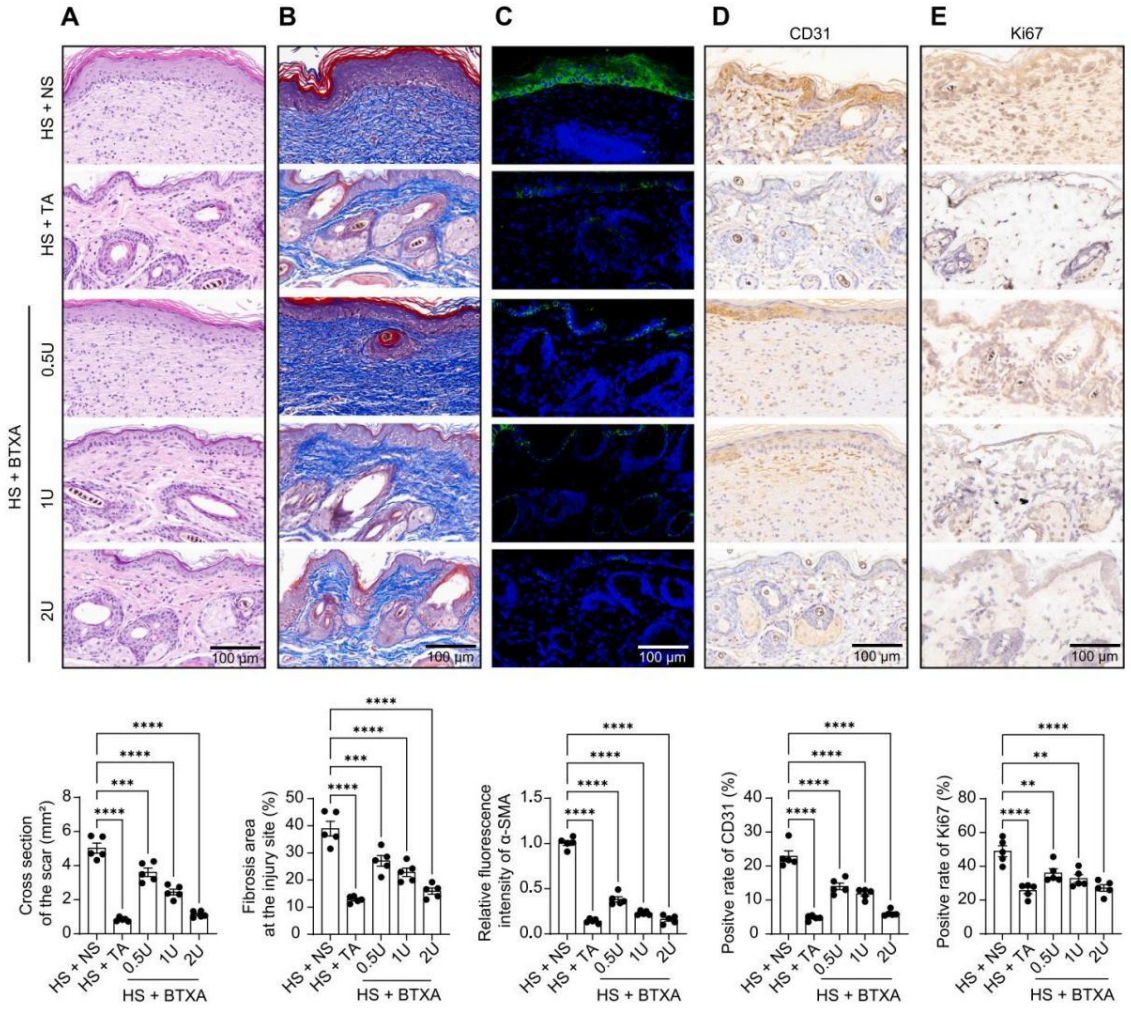

Fig. 1. BTXA exerts an ameliorating effect on HS formation. A mouse model of HS was generated, followed by treatment with 0.5 U, 1 U, and 2 U of BTXA or 0.05 mL/g of the positive drug TA. A, pathological changes in the lesion (scar) tissues determined using HE staining ($F(4, 20) = 82.51$, $p < 0.0001$); B, collagen deposition and fibrosis in the lesion (scar) tissues determined using Masson's trichome staining ($F(4, 20) = 34.88$, $p < 0.0001$); C, the staining intensity of α-SMA in the scar tissues determined using immunofluorescence staining ($F(4, 20) = 291.9$, $p < 0.0001$); D-E, positive staining of CD31 ($F(4, 20) = 63.97$, $p < 0.0001$) and Ki67 ($F(4, 20) = 14.70$, $p < 0.0001$) in the scar tissues determined using IHC. Each group contained 5 mice. Differences were analyzed using one-way ANOVA (A-E), followed by Tukey's multiple comparisons test. $^{**}p < 0.01$, $^{***}p < 0.001$, $^{****}p < 0.0001$.

concentration was determined using the bicinchoninic acid method. The samples were separated using SDS-PAGE and transferred onto polyvinylidene fluoride membranes (FFP24, Beyotime). After blocking with 5 % skim milk at 25 °C for 2 h, the membranes were probed with the antibodies against Collagen I (Col) (1:5000, PA1–26204, Thermo Fisher Scientific), Tgfb1 (1:2000, MA5–44667, Thermo Fisher Scientific), α-smooth muscle actin (α-SMA, 1:1000, ab5694, Abcam), PARP14 (1:2000, 84,039–6-RR, ProteinTech Group, Chicago, IL, USA), CD206 (1:2000, MA5–32498, Thermo Fisher Scientific), SOCS2 (1:100, MA5–35776, Thermo Fisher Scientific), β-catenin (1:1000, AF0066, Beyotime), histone H3 (1:2000, AF7104, Beyotime), and GAPDH (1:2500, ab9485, Abcam) overnight at 4 °C. Following this, the membranes were washed and incubated with the secondary antibody (1:30,000, ab205718, Abcam) at 25 °C for 1 h. The protein bands were visualized using the enhanced chemiluminescence method. GAPDH protein immunoreactivity served as an internal control for whole-cell component proteins, whereas histone H3 served as an internal control for intranuclear proteins.

2.11. RNA-immunoprecipitation (RIP)

Wild-type PARP14-tagged protein recombinant plasmid (Flag-PARP14-WT) and mutant PARP14-tagged protein recombinant plasmid with mutation in the mRNA binding site (Flag-PARP14-MT) were constructed by Gene Optimal (Shanghai, China) and transfected into THP-1 cells by Lipofectamine 3000 (Thermo Fisher). After 48 h, the RIP kit (P1801S, Beyotime) was used. In brief, protein A/G agarose was incubated at 25 °C for 30 min with IgG (1:1000, ab172730, Abcam) or anti-

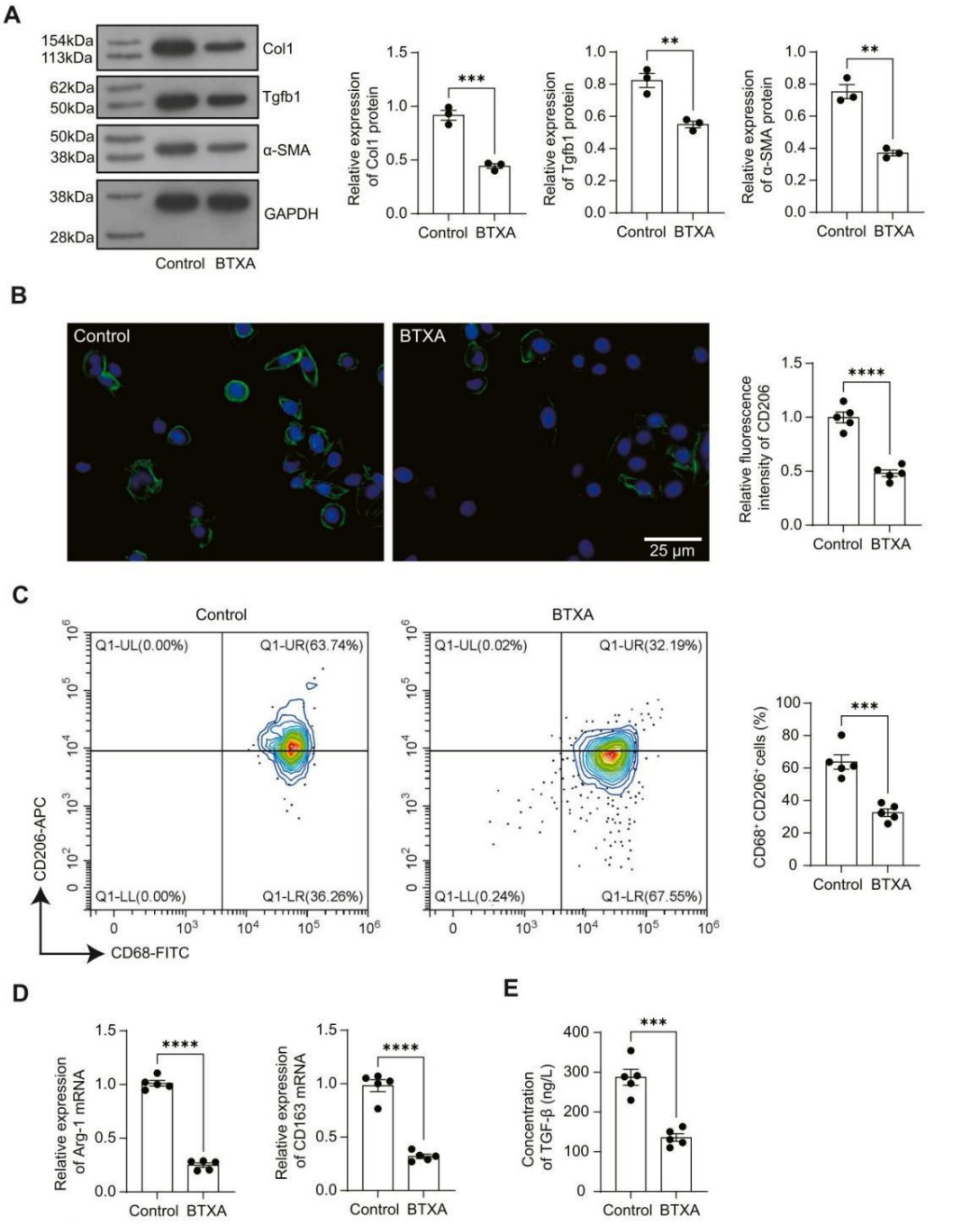

Fig. 2. BTXA treatment reduces M2 polarization of macrophages. PMA-stimulated THP-1 cells (M0 macrophages) were stimulated IL-4/IL-13, treated with BTXA or PBS (Control), which were then co-cultured with HDFs. A, protein levels of Col1, Tgfb1, and α-SMA in HDFs after co-culture determined using WB analysis; B, the staining intensity of CD206 in THP-1 cells determined using immunofluorescence staining; C, the proportion of $CD68^{+}CD206^{+}$ THP-1 cells determined using flow cytometry; D, mRNA expression of Arg-1 and CD163 in THP-1 cells detected using RT-qPCR; E, concentrations of TGF-β in the supernatant of THP-1 cells determined using ELISA. Five biological replicates were performed. All statistical graphs for WB were from three independent repeats. Differences were compared by the *t-tests* (A-E). $^{**}p < 0.01$, $^{***}p < 0.001$, $^{****}p < 0.0001$.

Flag (1:30, ab205606, Abcam). After incubation, the pre-bound protein A/G agarose was centrifuged at 1000 ×*g* for 1 min at 4 °C, and the supernatant was removed. A volume of 270 μL of THP-1 cell lysate was added to the antibody-prebound protein A/G agarose, mixed by inversion, and incubated on a shaker at 4 °C for 4 h. The RNA-protein complexes were then washed and incubated with proteinase K digestion buffer. Finally, RNA was purified using the RNAeasy Animal RNA Isolation Kit (R0027, Beyotime). The enrichment of SOCS2 RNA was determined by RT-qPCR.

2.12. RNA pull-down assay

The amplified wild-type SOCS2 mRNA (SOCS2-WT) and protein-binding site mutant SOCS2 mRNA (SOCS2-MT) were labeled with desulfated biotin using the Pierce RNA 3′-End Desthiobiotinylation Kit (20,163, Thermo Fisher Scientific). Subsequently, an RNA pull-down assay was performed using the Pierce Magnetic RNA-Protein Pull-Down Kit (20,164, Thermo Fisher Scientific). A total of 50 pmol of biotinylated SOCS2 was mixed with 2 mg of protein lysate and 50 μL of magnetic streptavidin beads. After incubation and washing three times, the streptavidin beads were boiled, and the samples were prepared for WB analysis.

2.13. mRNA stability assay

SOCS2 mRNA stability was assessed using the actinomycin D method. THP-1 cells overexpressing PARP14 were plated in six-well plates (5×10^5 cells/well). The cells were exposed to 2 μg/mL actinomycin D (SBR00013, Sigma-Aldrich) for 24 h, and RNA was collected at specified time points (0, 4, 8 h). The remaining RNA levels were analyzed using RT-qPCR and normalized to the 0-h value.

2.14. Immunofluorescence assay

For tissues, the mouse scar tissue sections were deparaffinized and rehydrated, followed by heat-induced antigen retrieval in citrate buffer (pH = 6.0) for 10 min. The samples were then incubated with the α-SMA antibody (1:500, ab124964, Abcam) overnight at 4 °C. The sections were washed three times with PBS and labeled with AlexaFluor 488-conjugated goat anti-rabbit IgG (1:250, A-11008, Thermo Fisher Scientific). After nuclear staining using 4′, 6-diamidino-2-phenylindole (DAPI), the images were acquired under a fluorescence microscope.

For cells, 5×10^5 THP-1 cells or HDFs after co-culture were seeded in six-well plates and fixed with 4 % paraformaldehyde for 30 min. The cells were washed and blocked with PBS containing 5 % goat serum. Subsequently, the cells were incubated with antibodies against CD206 (1:300, MA5–32498, Thermo Fisher Scientific), α-SMA (1:500, ab124964, Abcam), or Col1 (1:1000, PA1–26204, Thermo Fisher Scientific) overnight at 4 °C, followed by incubation with either Alexa Fluor 660-conjugated (1:1000, A-21074, Thermo Fisher) or Alexa Fluo 488-conjugated (1:250, A-11008, Thermo Fisher) secondary antibodies at 25 °C for 15 min. The cells were washed again three times for 15 min each with 5 % PBST. After drying, the cells were counterstained with DAPI, and the images were acquired under a fluorescence microscope.

2.15. Flow cytometry

The expression of the macrophage surface marker CD206 was assessed using flow cytometry. THP-1 cells were treated with rat anti-human CD16/CD32 (ab25235, Abcam) to block surface Fc receptors, followed by incubation with APC-conjugated mouse anti-human CD206 (17–2069-42, Thermo Fisher Scientific) and FITC-conjugated mouse anti-human CD68 (333,805, BioLegend, San Diego, CA, USA) in the dark. The cells were analyzed by flow cytometry using a flow cytometer.

2.16. TOP/FOP flash

The TOP Flash reporter gene plasmid (D2501, Beyotime) containing the TCF/LEF binding site sequence was used to assay the transcriptional regulatory activity of β-catenin, and the FOP Flash reporter gene plasmid (D2503, Beyotime) with the mutated TCF/LEF binding site sequence was used as a negative control. The above plasmids were transfected into cells by Lipofectamine 3000 and detected by the Firefly Luciferase Reporter Gene Assay Kit (RG005, Beyotime) after 48 h. The luciferase activity of TOP flash was standardized according to TOP flash.

2.17. Statistical analysis

Measurement data collected from a minimum of three biological replicates were analyzed utilizing Prism 8.0.2 (GraphPad, La Jolla, CA, USA). All data are expressed as mean ± standard error of the mean. The normal distribution of the data was verified by the Shapiro-Wilk test. Comparisons between groups were made using the *t-test*, or using one-way or two-way analysis of variance (ANOVA) with Tukey's post-hoc test, as appropriate. A *p*-value of <0.05 was deemed statistically significant.

3. Results

3.1. BTXA exerts an ameliorating effect on HS formation

First, a mouse model of HS was established, followed by treatment with 0.5 U, 1 U, and 2 U of BTXA or 0.05 mL/g of the positive drug TA to the lesions. HE staining results revealed that BTXA and TA treatment reduced dermal thickness and epidermal hyperplasia, decreased cell numbers, increased the number of dermal appendages, and significantly decreased the scar cross-sectional area in mice (Fig. 1A). Following BTXA and TA treatment, collagen deposition in the scars was also reduced, and the fibrotic area at the injury site was diminished (Fig. 1B). Immunofluorescence analysis showed that the relative fluorescence intensity of α-SMA, a marker of myofibroblasts and indicative of collagen matrix contraction ability, was significantly reduced in the scar tissues of mice following BTXA or TA treatment (Fig. 1C). Additionally, the IHC assay revealed that the levels of CD31 and Ki67, marker proteins of angiogenesis and proliferation, respectively, were significantly reduced in the scar tissue of mice receiving BTXA or TA treatment (Fig. 1D-E). These results demonstrate that both BTXA and TA have therapeutic effects on HS. Regarding the BTXA doses, a more pronounced ameliorating effect was observed at a dose of 2 U BTXA treatment. Therefore, this dose was selected for subsequent experiments.

3.2. BTXA treatment reduces M2 polarization of macrophages

It has been well established that M2 macrophages have a pro-fibrogenic effect, contributing to the formation of proliferative scars [38]. To investigate whether BTXA affects M2 macrophages, we generated M2 macrophages by exposing PMA-stimulated THP-1 cells (M0 macrophages) to IL-4/IL-13, which were then treated with 30 U/mL BTXA. A co-culture system of HDFs and the induced M2 macrophages was established. WB analysis revealed that the BTXA treatment significantly reduced the scar formation-related proteins Col1, Tgfb1, and α-SMA in HDFs following the M2 macrophage stimulation (Fig. 2A). Immunofluorescence staining revealed a significant reduction in the content of the M2 macrophage marker CD206 in THP-1 cells after BTXA treatment (Fig. 2B). This trend was validated by the flow cytometric analysis (Fig. 2C). Consistently, RT-qPCR results showed reduced expression of M2 macrophage-related genes Arg-1 and the surface marker CD163 in THP-1 cells following BTXA treatment (Fig. 2D). Furthermore, ELISA results demonstrated that the TGF-β levels were significantly decreased in the supernatant of THP-1 cells following BTXA treatment (Fig. 2E).

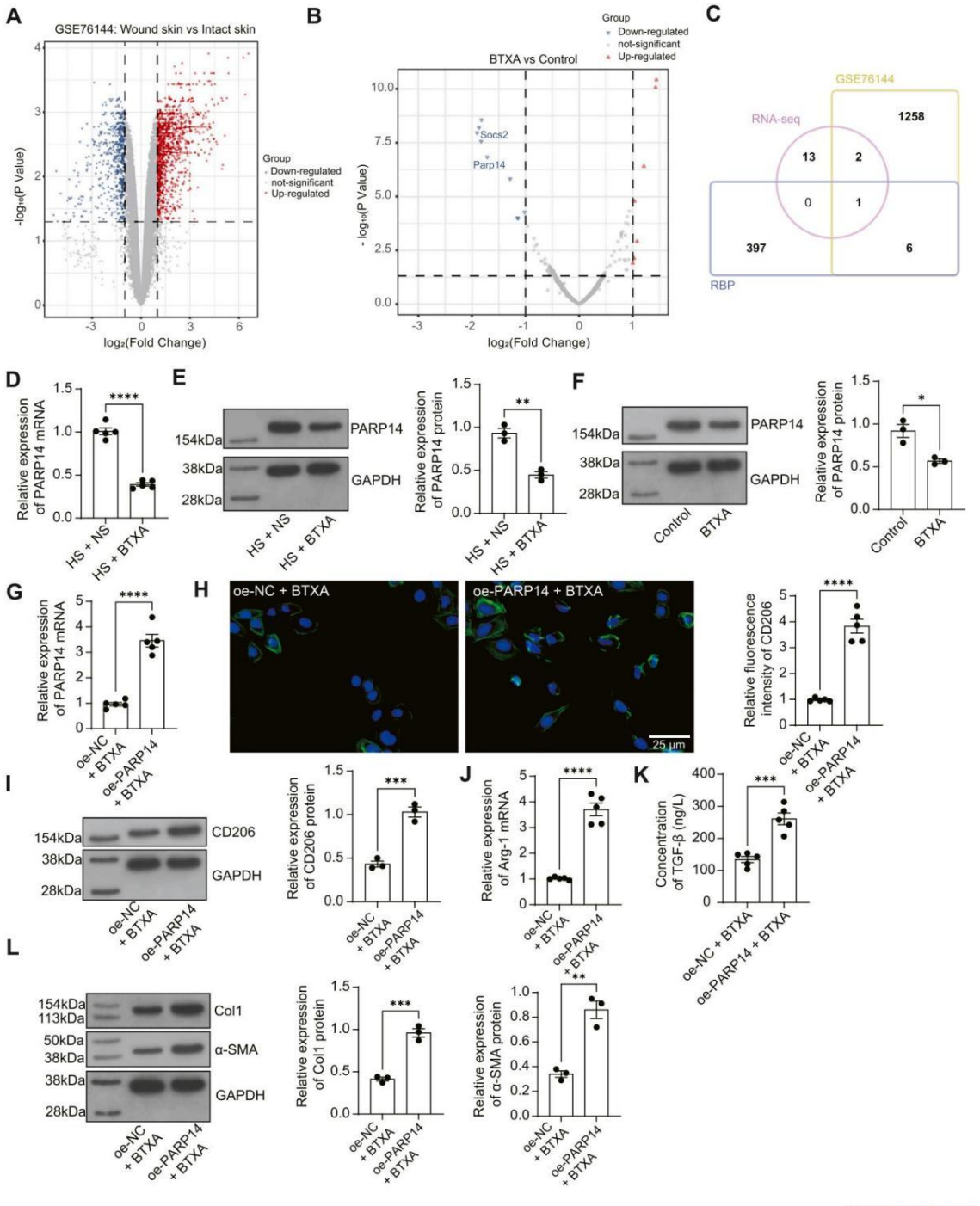

(caption on next page)

Fig. 3. BTXA suppresses M2 macrophages by downregulating PARP14. A, DEGs between wound skin and intact skin identified using the GSE76144 dataset; B, RNA-seq analysis on macrophage samples from the back skin of mice treated with 30 U/mL BTXA and those from control mice; C, an intersection analysis of DEGs from GSE76144 dataset and our RNA-seq analysis, and *Mus musculus* RBP from the RBPDB; D-E, mRNA (D) and protein (E) expression of PARP14 in the scar tissues of mice determined using RT-qPCR and WB assay, respectively; F, PARP14 protein level in THP-1 cells with or without BTXA treatment determined using WB analysis. THP-1 cells were infected with oe-PARP14 lentivirus and then with PMA, IL-4/IL-13, and treated with BTXA. G, mRNA expression of PARP14 in THP-1 cells determined using RT-qPCR; H, staining intensity of CD206 in THP-1 cells determined using immunofluorescence staining; I, protein level of CD206 in THP-1 cells determined using WB analysis; J, mRNA expression of Arg-1 in THP-1 cells detected using RT-qPCR; K, concentrations of TGF-β in the supernatant of THP-1 cells determined using ELISA; L, protein levels of Col1 and α-SMA in HDFs after co-culture with the THP-1 cells determined using WB analysis. For animal experiments, each group contained 5 mice; for cell experiments, five biological replicates were performed. All statistical graphs for WB were from three independent repeats. Differences were compared by the *t-tests* (D-L). $^{*}p < 0.05$, $^{**}p < 0.01$, $^{***}p < 0.001$, $^{****}p < 0.0001$.

3.3. BTXA suppresses M2 macrophages by downregulating PARP14

To investigate the molecular mechanisms through which BTXA alleviates hypertrophic scarring, we used the GEO2R tool from GEO Datasets with a filter of $p < 0.05$ and $|\text{Log2FC} > 1|$ to analyze DEGs between wound skin and intact skin in dataset GSE76144 (Fig. 3A). Similarly, we performed an RNA-seq analysis on macrophage samples from the back skin of mice treated with 30 U/mL BTXA and control mice, using the same filtering criteria (Fig. 3B). Many disease-related genes encode RBPs, and dysfunction of RBPs can lead to multiple forms of cellular dysfunction by disrupting RNA metabolism [13]. Therefore, we downloaded *Mus musculus* RBPs from RBPDB (http://rbpdb.ccbr.utoronto.ca/) and identified a unique intersecting RBP, PARP14, between DEGs from GSE76144 and RNA-seq results (Fig. 3C). In the GSE76144 dataset, PARP14 (ID = 10,439,249) was significantly upregulated in wound skin samples (Log2FC = 2.19). Notably, the RNA-seq data revealed that PARP14 expression in macrophages was significantly downregulated (Log2FC = −1.71) following BTXA treatment of wound skin. Therefore, we hypothesize that BTXA inhibits M2 polarization of macrophages and prevents fibrosis in HS formation by downregulating PARP14 expression.

Importantly, RT-qPCR and WB results revealed that the PARP14 mRNA expression in scar tissue was significantly reduced following BTXA treatment (Fig. 3D-E). Additionally, WB analysis revealed that BTXA treatment led to a significant downregulation of PARP14 protein expression in M2-polarized THP-1 cells (Fig. 3F), confirming the ability of BTXA to reduce PARP14 expression.

To explore the functional role of PARP14 in macrophage M2 polarization, we infected THP-1 cells with oe-PARP14 lentivirus and then had them stimulated with PMA, IL-4/IL-13, and BTXA. RT-qPCR confirmed efficient overexpression of PARP14 in THP-1 cells (Fig. 3G). Immunofluorescence staining (Fig. 3H) and WB (Fig. 3I) showed that CD206 content was significantly increased in THP-1 cells upon PARP14 overexpression. Moreover, the PARP14 overexpression significantly increased Arg-1 expression in THP-1 cells even in the presence of BTXA treatment (Fig. 3J), accompanied by increased TGF-β levels (Fig. 3K). Furthermore, PARP14 overexpression in THP-1 cells led to increased protein levels of Col1 and α-SMA in the co-cultured HDFs (Fig. 3L). This evidence indicates that the HS-ameliorating effects are attributed to PARP14 downregulation.

3.4. PARP14 overexpression negates the treatment effect of BTXA on mice with HS

The oe-PARP14 and oe-NC lentiviruses were administered to HS mice, accompanied by BTXA treatment. After animal sacrifice, the WB assay confirmed that PARP14 protein expression was enhanced by oe-PARP14 (Fig. 4A). This condition led to increased dermal thickness and epidermal hyperplasia, with a higher cell count and reduced number of dermal appendages, resulting in a significantly larger scar cross-sectional area (Fig. 4B). Moreover, the collagen deposition in HS scars was augmented upon PARP14 overexpression (Fig. 4C). Additionally, this oe-PARP14 administration significantly increased the protein level of α-SMA in the mouse scar tissues (Fig. 4D), accompanied by increased staining of CD31 and Ki67 (Fig. 4E-F). RT-qPCR analysis of M2 macrophage-related genes in HS scar tissue revealed that BTXA treatment reduced Arg-1 and TGF-β expression, which was restored by PARP14 overexpression (Fig. 4G). IHC assay showed that the positive cell rate of CD163 was decreased following BTXA treatment but restored following PARP14 overexpression (Fig. 4H).

3.5. BTXA inhibits PARP14 expression to reduce SOCS2 mRNA stability

Given that PARP14 functions as an RBP, we downloaded mRNAs interacting with the PARP14 protein from RNAInter (http://www.rnainter.org/) and identified a unique intersection with DEG from GSE76144 and RNA-seq results: SOCS2 (Fig. 5A). Additionally, using the PRIdictor tool from RNAInter (Fig. 5B-C), we found the existence of interaction sites between the PARP14 protein and SOCS2 mRNA. Interestingly, SOCS2 (ID = 10,394,674) was upregulated after skin injury (Log2FC = 1.09) according to the GSE76144 data, but significantly downregulated in mouse macrophages after BTXA treatment (Log2FC = −1.83) according to the RNA-seq results.

In THP-1 cells, the SOCS2 mRNA expression was found to be downregulated by BTXA treatment but restored following PARP14 overexpression (Fig. 5D). The presence of PARP14 protein in THP-1 cells pulled down by Bio-SOCS2-WT was confirmed by RNA pull-down and WB assay analyses, whereas it was absent in Bio-SOCS2-MT probe, in which the potential PARP14 binding site on the mRNA was mutated (Fig. 5E). THP-1 cells were transfected with Flag-PARP14-WT or a tagged recombinant protein with a mutation in the mRNA binding site (Flag-PARP14-MT). RIP-qPCR analysis demonstrated that Flag-PARP14-WT was able to pull down SOCS2 mRNA in THP-1 cells, whereas Flag-PARP14-MT was unable to pull down SOCS2 mRNA (Fig. 5F). Therefore, PARP14 protein and SOCS2 mRNA bound in a site-dependent manner in THP-1 cells.

Overexpression of PARP14 was found to retard SOCS2 mRNA degradation by RT-qPCR analysis (Fig. 5G), indicating that PARP14 enhances SOCS2 mRNA stability.

3.6. SOCS2 silencing attenuates M2 polarization induced by PARP14 overexpression

THP-1 cells stably transfected with oe-PARP14 were further administered three shRNAs of SOCS2 (sh-SOCS2 #1, #2, and #3), followed by PMA and IL-4/IL-13 stimulation and BTXA treatment. RT-qPCR results indicated successful downregulation of SOCS2 expression by all three shRNAs (Fig. 6A). Among these, sh-SOCS2 #2 and sh-SOCS2 #3, which demonstrated higher knockdown efficiency, were selected for subsequent experiments. WB (Fig. 6B) and flow cytometry (Fig. 6C) analyses revealed a decrease in the expression of CD206 in THP-1 cells following SOCS2 knockdown, and RT-qPCR demonstrated that either sh-SOCS2 #2 or sh-SOCS2 #3 significantly reduced the expression of Arg-1 in these cells (Fig. 6D). ELISA analysis showed a significant decrease in TGF-β levels in the THP-1 cell supernatants in the presence of sh-SOCS2 knockdown (Fig. 6E). Additionally, in the co-culture system, the SOCS2 silencing in THP-1 cells was found to reduce the protein level and immunofluorescence staining intensity of Col1 and α-SMA in HDFs (Fig. 6F-G).

BTXA treatment inhibited nuclear β-catenin expression as detected

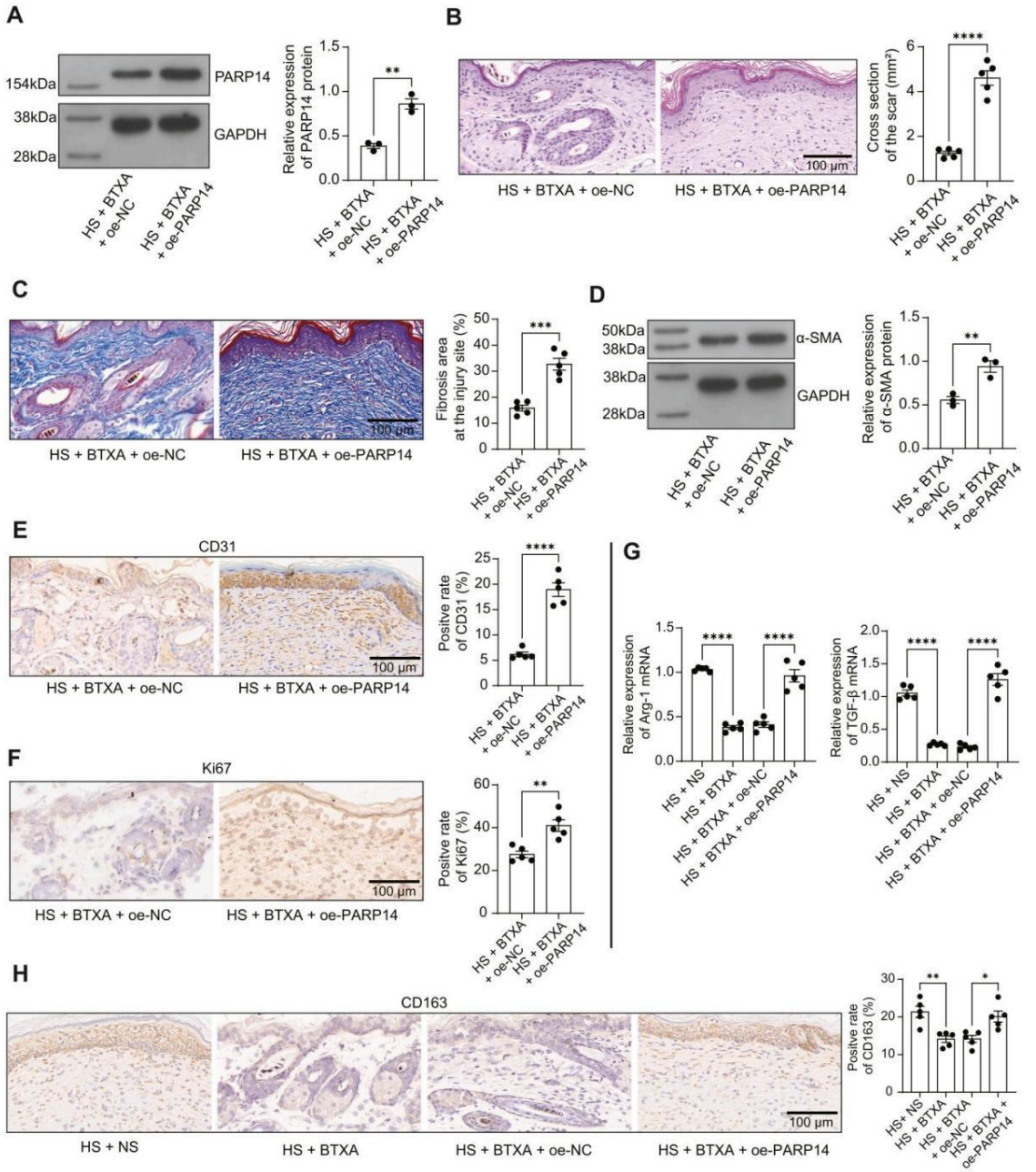

Fig. 4. PARP14 overexpression negates the treatment effect of BTXA on mice with HS. Mice with HS were administered oe-PARP14 and oe-NC lentiviruses, accompanied by BTXA treatment. A, PARP14 protein expression in the scar tissues determined using WB analysis; B, pathological changes in the scar tissues determined using HE staining; C, collagen deposition and fibrosis in the scar tissues determined using Masson's trichome staining; D, the protein level of α-SMA in the scar tissues determined using WB analysis; *E*-F, positive staining of CD31 (E) and Ki67 (F) in the scar tissues determined using IHC; G, mRNA expression of Arg-1 ($F(3, 16) = 76.86$, $p < 0.0001$) and TGF-β ($F(3, 16) = 104.8$, $p < 0.0001$) in the scar tissues determined using RT-qPCR; H, positive staining of CD163 ($F(3, 16) = 9.927$, $p = 0.0006$) in the scar tissues determined using IHC. Each group contained 5 mice. All statistical graphs for WB were from three independent repeats. Differences were analyzed using the *t-tests* (A-F) or one-way ANOVA (G-H), followed by Tukey's multiple comparisons test. $^{*}p < 0.05$, $^{**}p < 0.01$, $^{***}p < 0.001$, $^{****}p < 0.0001$.

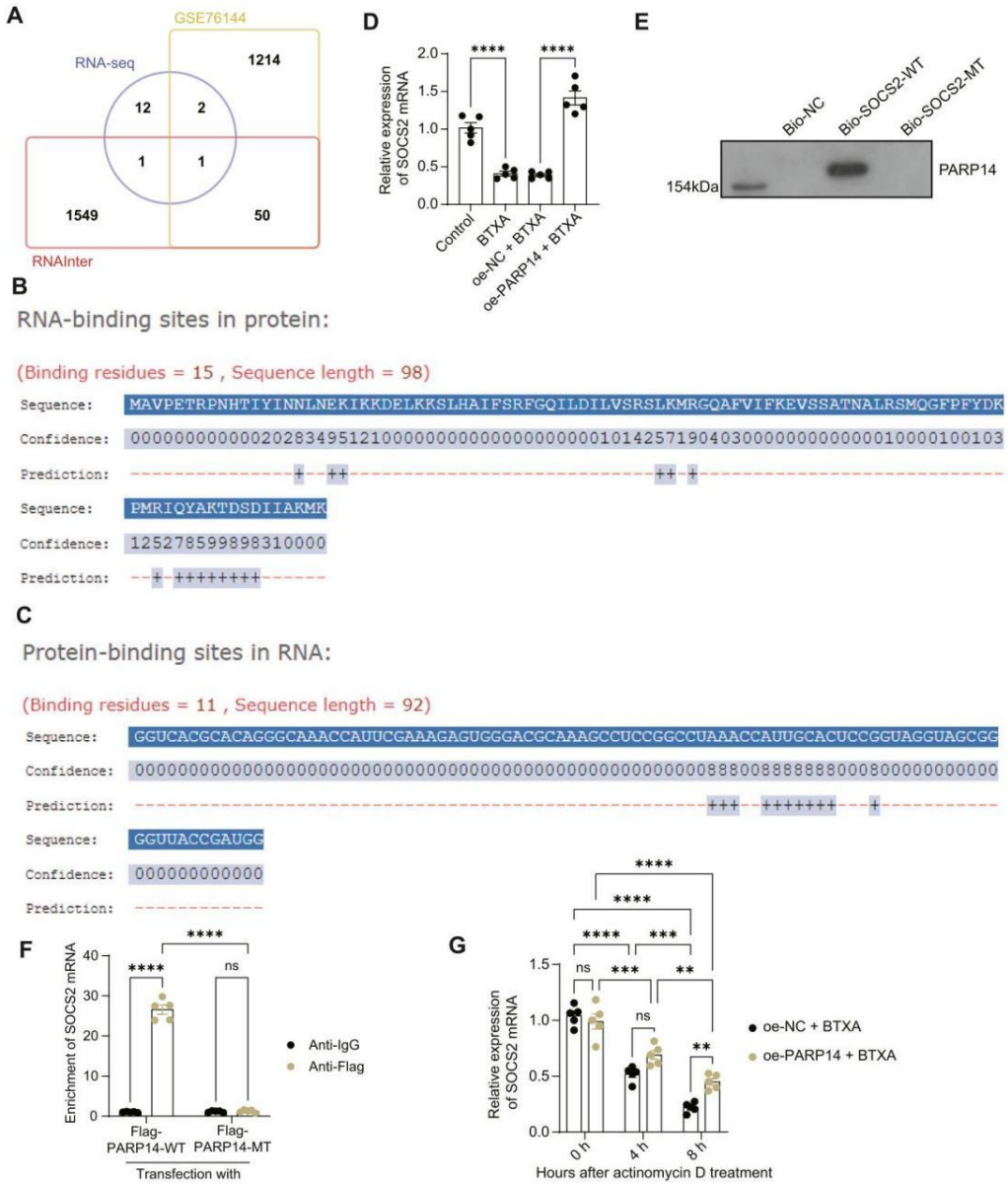

Fig. 5. BTXA inhibits PARP14 expression to reduce SOCS2 mRNA stability. A, an intersection between mRNA interacting with PARP14 protein (*Mus musculus*) predicted from the RNA Inter system, DEGs from the GSE76144 dataset, and DEGs from RNA-seq results; B—C, binding sites between PARP14 protein and SOCS2 mRNA predicted using the PRIdictor tool and RNAInter system; D, SOCS2 mRNA expression ($F(3, 16) = 67.95$, $p < 0.0001$) in THP-1 cells following different treatments determined using RT-qPCR; E, binding between SOCS2 and the PARP14 protein determined using RNA pull-down assay; F, binding between PARP14 protein and SOCS2 mRNA in THP-1 cells determined using RIP-RT-qPCR assays ($F(1, 16) = 485.7$, $p < 0.0001$); G, SOCS2 mRNA stability ($F(2, 24) = 6.467$, $p = 0.0057$) in THP-1 cells in the presence of actinomycin D treatment. Five biological replicates were performed. Differences were analyzed using one-way (D) or two-way (F-G) ANOVA, followed by Tukey's multiple comparisons test. $^{**}p < 0.01$, $^{***}p < 0.001$, $^{****}p < 0.0001$.

by WB, and overexpression of PARP14 promoted nuclear expression of β-catenin, which was significantly reversed by knocking down SOCS2 (Fig. 6H). The TOP/FOP flash assay directly demonstrated that BTX1 inhibited the transcriptional regulatory activity of β-catenin, as evidenced by attenuated luciferase activity of TOP flash, and PARP14 rescued β-catenin signaling in a SOCS2-dependent manner (Fig. 6I).

3.7. SOCS2 silencing reduces M2 macrophages and attenuates HS in mice

The sh-SOCS2 #2 with the highest knockdown efficiency was

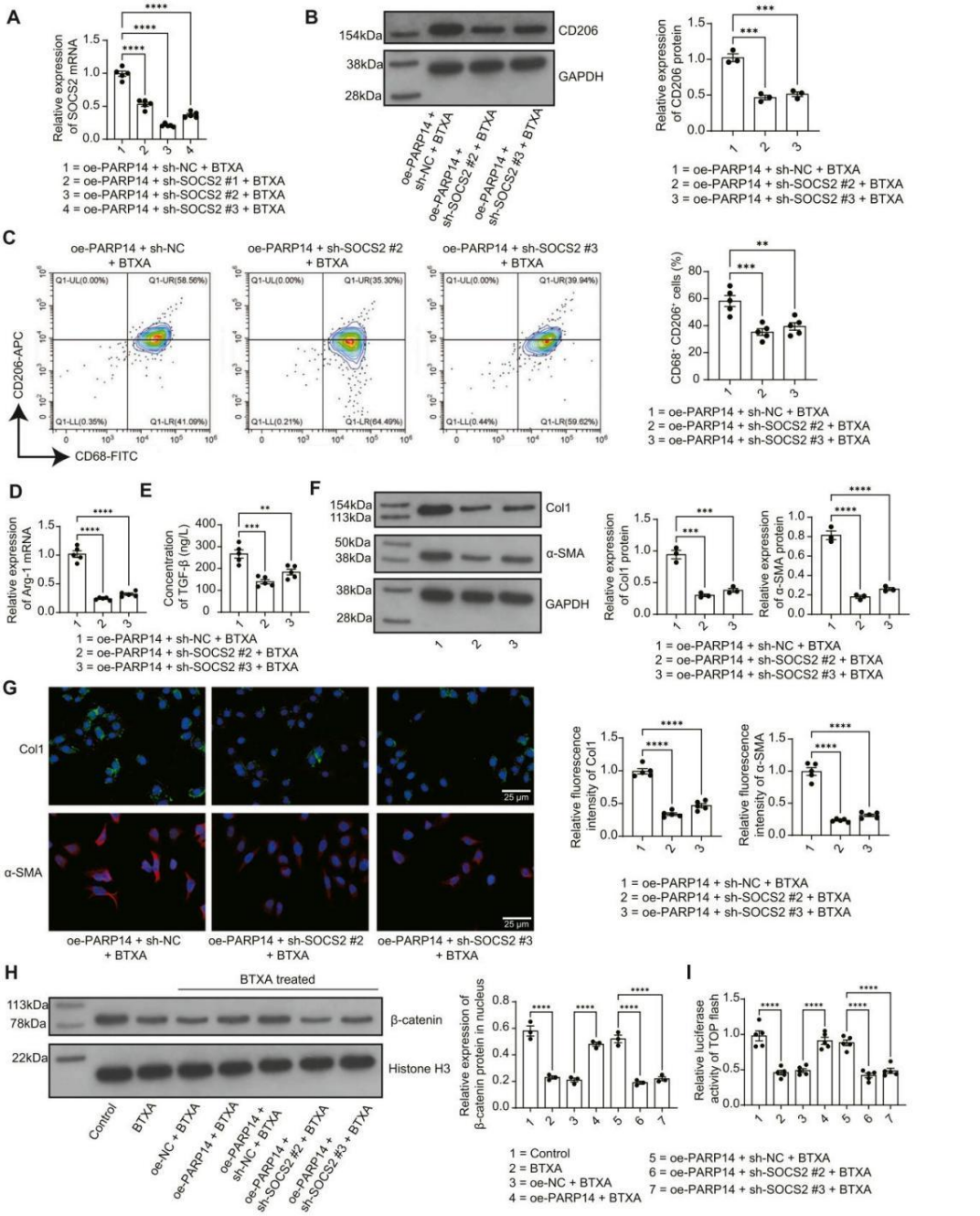

(caption on next page)

Fig. 6. SOCS2 silencing attenuates M2 polarization of macrophages induced by PARP14 overexpression. THP-1 cells stably transfected with oe-PARP14 were further administered three shRNAs of SOCS2 (sh-SOCS2 #1, #2, and #3) and then with PMA, IL-4/IL-13, and treated with BTXA. A, mRNA expression of SOCS2 ($F(3, 16) = 155.2$, $p < 0.0001$) in THP-1 cells determined using RT-qPCR; B, protein level of CD206 ($F(2, 6) = 57.60$, $p = 0.0001$) in THP-1 cells determined using WB analysis; C, proportion of $CD68^+$ $CD206^+$ THP-1 cells ($F(2,12) = 14.86$, $p = 0.0006$) determined using flow cytometry; D, mRNA expression of Arg-1 ($F(2, 12) = 148.9$, $p < 0.0001$) in THP-1 cells detected using RT-qPCR; E, concentrations of TGF-β ($F(2, 12) = 20.52$, $p = 0.0001$) in the supernatant of THP-1 cells determined using ELISA kits; F, protein levels of Col1 ($F(2, 6) = 63.10$, $p < 0.0001$) and α-SMA ($F(2, 6) = 144$, $p < 0.0001$) in the co-cultured HDFs determined using WB analysis; G, staining intensity of Col1 ($F(2, 12) = 122.6$, $p < 0.0001$) and α-SMA ($F(2, 12) = 130.7$, $p < 0.0001$) in the co-cultured HDFs determined using immunofluorescence staining; H, β-catenin expression ($F(6, 14) = 63.20$, $p < 0.0001$) in the nucleus of THP-1 cells determined using WB analysis; I, transcriptional regulatory activity of β-catenin ($F(6, 28) = 33.81$, $p < 0.0001$) in THP-1 cells determined using TOP/FOP flash assay. Five biological replicates were performed. All statistical graphs for WB were from three independent repeats. Differences were compared by one-way ANOVA (A-I), followed by Tukey's multiple comparisons test. $^{**}p < 0.01$, $^{***}p < 0.001$, $^{****}p < 0.0001$.

selected for use in HS mice along with oe-PARP14, followed by BTXA treatment. The WB assay revealed that the protein expression of SOCS2 in the scar tissues was reduced by BTXA treatment, increased upon PARP14 overexpression, but reduced again by the additional administration of sh-SOCS2 (Fig. 7A). The SOCS2 knockdown significantly reduced the scar cross-sectional area in mice (Fig. 7B) and inhibited collagen deposition in the scars of HS mice (Fig. 7C). The fluorescence intensity of α-SMA in the scar tissue was significantly reduced by the SOCS2 knockdown as well (Fig. 7D). IHC assay showed that the positive staining of CD31 and Ki67 in the scar tissues of HS mice was decreased following SOCS2 knockdown (Fig. 7E-F). Additionally, RT-qPCR analysis revealed that SOCS2 knockdown inhibited the expression of Arg-1 and TGF-β in the scar tissues of mice (Fig. 7G). The IHC assay further showed that sh-SOCS2 intervention inhibited the positive staining of CD163 in the scar tissues of mice (Fig. 7H).

WB assay (Fig. 7I) was performed on macrophages isolated from scar tissues of mice in each group, and it was observed that BTXA treatment inhibited the intranuclear expression of β-catenin in scar tissue-derived macrophages. The inhibitory effect of BTXA on β-catenin was reversed by overexpression of PARP14, whereas combined knockdown of SOCS2 resulted in a blockade of β-catenin expression in the nucleus. TOP/FOP flash confirmed that the intracellular β-catenin pathway activity was in line with the changes in β-catenin expression in the nucleus (Fig. 7J).

4. Discussion

Research has shown that depleting systemic macrophages during the acute phase of wound healing can enhance recovery, while simultaneously reducing wound contraction, the presence of myofibroblasts, collagen production, and the hypertrophic characteristics of fibers in mice with human skin grafts [38]. This underscores the critical role of macrophages in the development of HS. In this study, we present a novel finding regarding BTXA, demonstrating its ability to diminish the transition of macrophages to the M2 phenotype, thereby contributing to the mitigation of HS.

As the most commonly applied and commercially available type of BTX, BTXA has been frequently investigated as an effective regimen to treat HS. For instance, intralesional administration of BTXA has been reported to exhibit a more pronounced effect than corticosteroid or placebo in HS prevention and reduction [2]. BTXA injection reduced the expression of vascular endothelial growth factor and suppressed angiogenesis to suppress HS formation in rabbit ears [37]. Similar observations were found by Yang et al., with an immediate postoperative injection of BTXA suppressed fibroblast proliferation, angiogenesis, and TGF-β1 expression in a dose-dependent manner [33]. Li and colleagues ascribed the HS-suppressing effect of BTXA to the suppression of TGF-β1/Smad and extracellular signal-related kinase signaling pathways [18]. Regarding the function of BTXA in macrophages, previous evidence has shown that BTXA administration reduced injury-activated neuronal function for antinociceptive action, which involves the silencing of microglia and macrophages [19]. More interestingly, BTXA has been demonstrated to induce proinflammatory mediators, such as nitric oxide and tumor necrosis factor-alpha, in mouse RAW264.7 macrophages; however, it suppressed excessive production of these factors in RAW264.7 cells upon lipopolysaccharide [14]. This evidence indicates that BTXA possibly mediates proper pro-inflammatory (M1) activation of macrophages but reduces overzealous inflammation, which is fundamental for the proper wound-healing process [32]. However, less has been concerned in terms of the role of BTXA in macrophage polarization in the context of HS. Importantly, we found that the administration of BTXA significantly reduced the population of M2 macrophages and the M2 markers in the HS lesions as well as in IL-4/IL-13-induced macrophages *in vitro*. This evidence suggests the suppression of M2 macrophages as an important aspect of the effect of BTXA on HS inhibition.

Regarding the downstream cascades, our RNA-seq analysis results demonstrated PARP14 and SOCS2 as two genes significantly suppressed by BTXA in the skin tissues of HS mice, which were initially upregulated in the wound skin tissues. Interestingly, PARP14 silencing has been reported to suppress the expression of anti-inflammatory genes and phosphorylation of signal transducer and activator of transcription 6, thus reducing M2 polarization of macrophages induced by IL-4 [10]. Similarly, an inhibitor of PARP14 has been found to suppress IL-4-induced immunosuppressive genes in macrophages [24]. Sturniolo et al. demonstrated that macrophages isolated from PARP14-knockout mice have a substantially weakened ability to acquire an M2 phenotype [27]. Here, overexpression of PARP14 negated the effects of BTXA on mice and THP-1 cells, promoting the expression of M2 cytokines and markers and contributing to increased collagen deposition and fibrosis. Moreover, PARP14 has been found to enhance the mRNA stability of the cyclin D1 gene to trigger cell cycle progression [22]. Here, we observed that the PARP14 protein interacted with the SOCS2 mRNA to enhance its stability. While the effect of SOCS2 on HS has not been investigated, SOCS2 plays a significant role in inducing M2 polarization of macrophages by upregulating IL-10 levels in the intestinal ischemia-reperfusion injury [35]. Our results demonstrated that in the presence of BTXA treatment and PARP14 overexpression, the additional SOCS2 silencing significantly weakened the M2 polarization of macrophages in mice and cell culture systems, leading to reduced collagen deposition and fibrosis, thus reducing HS through blocking the β-catenin signaling.

Our research mainly focused on the role of BTXA-mediated PARP14 inhibition in HS, but there were some limitations. Firstly, PARP14-deficient mice from ES cells heterozygous for a disruption of the 5'end of PARP14 genomic sequences have been used by Cho et al. [6]. It is now acknowledged that, in the absence of direct *in vivo* validation employing PARP14 knockout models, the causal relationship between PARP14 and the observed phenotypes remains inferential and based on correlative evidence. This finding underscores the necessity for subsequent studies to validate our conclusions using genetically modified animal models. Secondly, our current study reveals a downstream molecular signaling for BTXA to exert its function, *i.e.*, targeting the PARP14/SOCS2 axis. Since we screened out PARP14 as a target of BTXA using transcriptome sequencing, it is not yet known whether PARP14 is a direct target of BTXA or whether BTXA affects PARP14 expression through other signaling. For instance, BTXA could potentially alter the expression of microRNAs that target PARP14 mRNA, leading to changes in its expression [4,28]. Finally, while the results of the present study provide important mechanistic insights, their translational potential warrants

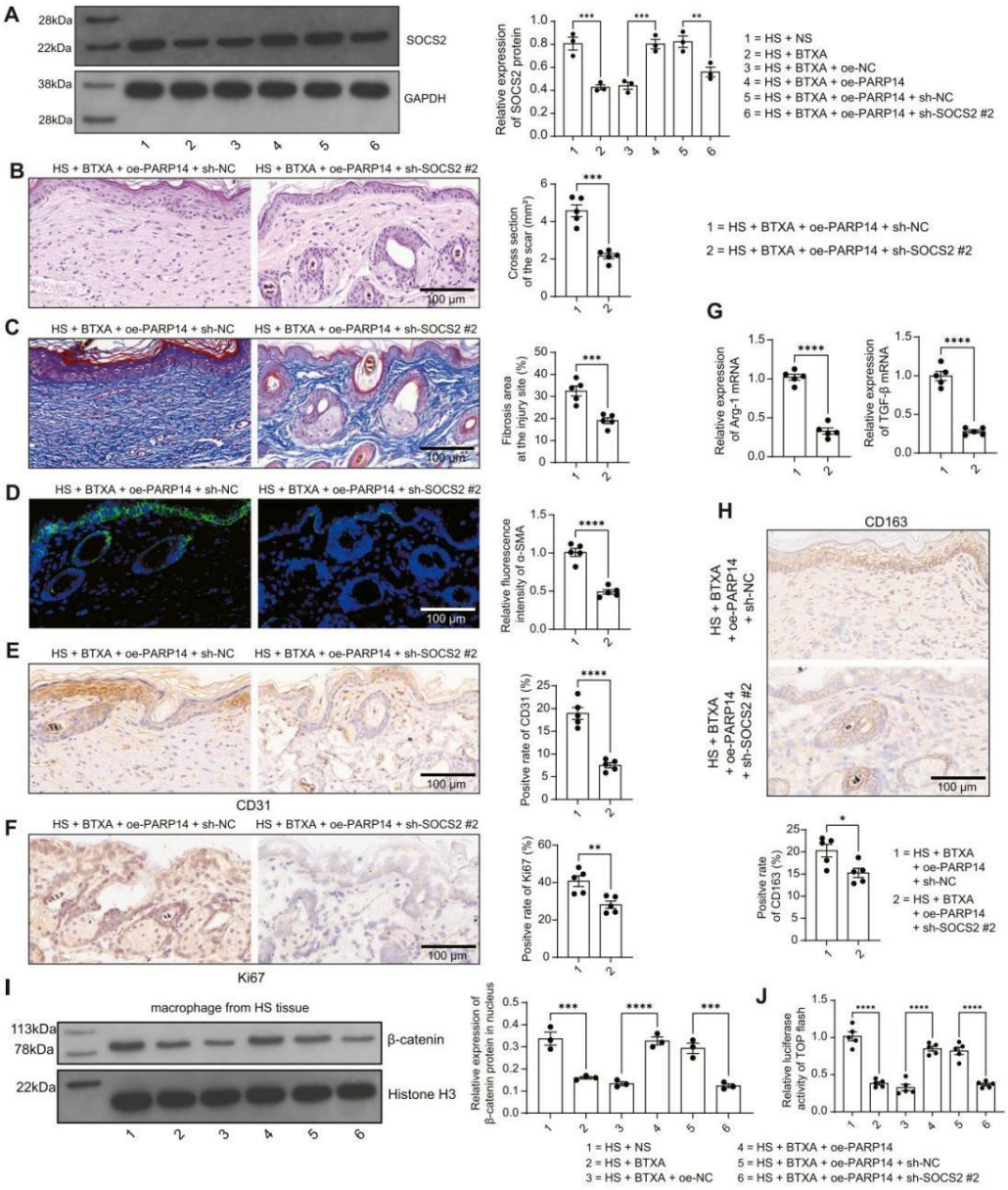

Fig. 7. SOCS2 silencing reduces M2 macrophages and attenuates HS in mice. Mice with HS were administered oe-PARP14 and sh-SOCS2 lentiviruses, accompanied by BTXA treatment. A, protein expression of SOCS2 ($F(5, 12) = 20.80$, $p < 0.0001$) in the scar tissues determined using WB analysis; B, pathological changes in the scar tissues determined using HE staining; C, collagen deposition and fibrosis in the scar tissues determined using Masson's trichome staining; D, relative fluorescence intensity of α-SMA in the scar tissue determined using immunofluorescence staining; *E*-F, positive staining of CD31 (E) and Ki67 (F) in the scar tissues determined using IHC; G, mRNA expression of Arg-1 and TGF-β in the scar tissues determined using RT-qPCR; H, positive staining of CD163 in the scar tissues determined using IHC; I, β-catenin expression ($F(5, 12) = 31.99$, $p < 0.0001$) in the nucleus of macrophages isolated from HS tissues determined using WB analysis; J, transcriptional regulatory activity of β-catenin ($F(5, 24) = 55.68$, $p < 0.0001$) in macrophages isolated from HS tissues determined using TOP/FOP flash assay. Each group contained 5 mice. All statistical graphs for WB were from three independent repeats. Differences were analyzed using the one-way ANOVA (A, I-J), followed by Tukey's multiple comparisons test or *t*-tests (B—H). $^{*}p < 0.05$, $^{**}p < 0.01$, $^{***}p < 0.001$, $^{****}p < 0.0001$.

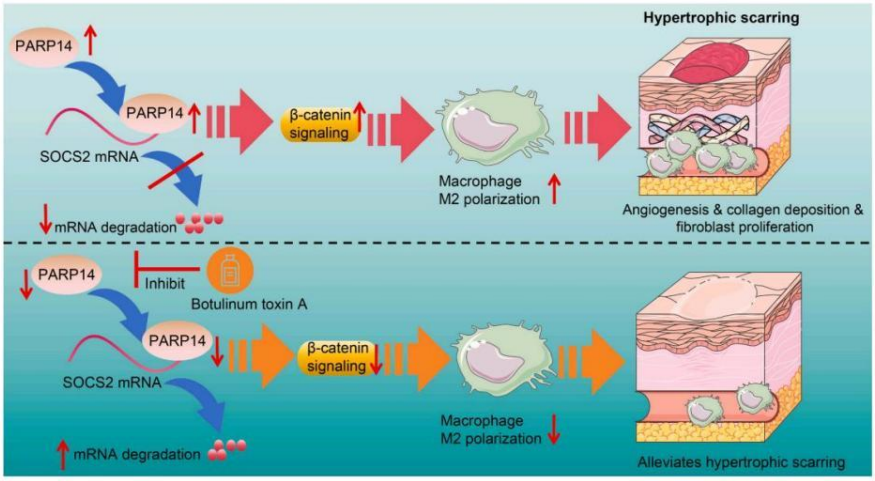

Fig. 8. Therapeutic effects of BTXA on HS. Dysregulation of PARP14 maintains β-catenin signaling-mediated macrophage M2 polarization by enhancing the stability of SOCS2 mRNA, leading to abnormal angiogenesis, collagen accumulation, and fibroblast proliferation in HS. BTXA inhibits macrophage M2 polarization and alleviates HS by inhibiting the expression of PARP14, facilitating SOCS2 mRNA degradation, and impairing β-catenin signaling.

further exploration. In particular, validation using clinical samples from patients with HS is essential to confirm the relevance of the PARP14/SOCS2 axis in human pathology. The findings of such studies could assist in determining the efficacy of BTXA or related modulators in the context of clinical treatment protocols. Future research should also assess the safety, dosage, and delivery methods of BTXA in the context of scar modulation, ultimately bridging the gap between experimental findings and clinical application.

In conclusion, this study highlights the role of BTXA in alleviating HS formation by limiting M2 macrophages (Fig. 8). These effects are, at least partly, achieved through the inhibition of PARP14-mediated SOCS2 mRNA stabilization and the β-catenin signaling. These observations may provide novel insights into the functional mechanisms of BTXA in HS prevention or treatment.

Supplementary data to this article can be found online at https://doi.org/10.1016/j.bbamcr.2025.120003.

CRediT authorship contribution statement

Mohyeddin Ali: Writing – review & editing, Validation, Supervision, Software, Resources, Methodology, Investigation, Formal analysis, Data curation. **Bochao Xie:** Writing – review & editing, Validation, Supervision, Software, Methodology, Investigation, Formal analysis, Data curation. **Pengfei Li:** Writing – review & editing, Validation, Resources, Methodology, Investigation, Formal analysis, Data curation. **Shuwei Chen:** Writing – review & editing, Validation, Software, Resources, Methodology, Investigation, Formal analysis, Data curation. **Yao Lu:** Writing – review & editing, Validation, Supervision, Software, Methodology, Investigation, Formal analysis, Data curation. **Fazhi Qi:** Writing – review & editing, Validation, Software, Resources, Methodology, Investigation, Formal analysis, Data curation. **Ze Xiong:** Writing – review & editing, Validation, Resources, Project administration, Methodology, Formal analysis, Data curation. **Jianrui Li:** Writing – review & editing, Visualization, Validation, Supervision, Project administration, Methodology, Investigation, Data curation.

Declaration of competing interest

The authors declare that they have no known competing financial interests or personal relationships that could have appeared to influence the work reported in this paper.

Acknowledgements

We thank the National Natural Science Foundation of China (82172212, 82372518), the China University Research Innovation Fund - Digital Health Project (2023GY056), the International S&T Cooperation Program of Shanghai (24490710900), and the start-up grant from ShanghaiTech University (2023F0209-000-02) for funding support.

Data availability

All data in this study are available from the corresponding author on reasonable request.

References

[1] L. Beck, S. Coates, J. Gee, T. Hadfield, P. Jackson, P. Keim, L. Lindler, V. Olson, E. Ostlund, F. Roberto, J. Samuel, S. Sharma, S. Tallent, D. Wagner, Performance standards for biological threat agent assays for Department of Defense Applications, J. AOAC Int. 101 (2018) 1665–1708.
[2] M. Bi, P. Sun, D. Li, Z. Dong, Z. Chen, Intralesional injection of botulinum toxin type a compared with Intralesional injection of corticosteroid for the treatment of hypertrophic scar and keloid: a systematic review and Meta-analysis, Med. Sci. Monit. 25 (2019) 2950–2958.
[3] H.C. Chen, C.I. Yen, S.Y. Yang, C.J. Chang, J.Y. Yang, S.Y. Chang, S.S. Chuang, Y. C. Hsiao, Comparison of steroid and botulinum toxin type a monotherapy with combination therapy for treating human hypertrophic scars in an animal model, Plast. Reconstr. Surg. 140 (2017) 43e–49e.
[4] M. Chen, G. Hu, X. Zhou, Z. Peng, W. Wen, Hsa_circ_0016788 regulates hepatocellular carcinoma progression via miR-506-3p/poly-adenosine diphosphate-ribose polymerase, J. Gastroenterol. Hepatol. 36 (2021) 3457–3468.
[5] R.S. Chiang, A.A. Borovikova, K. King, D.A. Banyard, S. Lalezari, J.D. Toranto, K. Z. Paydar, G.A. Wirth, G.R. Evans, A.D. Widgerow, Current concepts related to hypertrophic scarring in burn injuries, Wound Repair Regen. 24 (2016) 466–477.
[6] S.H. Cho, S. Goenka, T. Henttinen, P. Gudapati, A. Reinikainen, C.M. Eischen, R. Lahesmaa, M. Boothby, PARP-14, a member of the B aggressive lymphoma family, transduces survival signals in primary B cells, Blood 113 (2009) 2416–2425.
[7] Y. Feng, Z.L. Sun, S.Y. Liu, J.J. Wu, B.H. Zhao, G.Z. Lv, Y. Du, S. Yu, M.L. Yang, F. L. Yuan, X.J. Zhou, Direct and indirect roles of macrophages in hypertrophic scar formation, Front. Physiol. 10 (2019) 1101.
[8] F.S. Frech, L. Hernandez, R. Urbonas, G.A. Zaken, I. Dreyfuss, K. Nouri, Hypertrophic scars and keloids: advances in treatment and review of established therapies, Am. J. Clin. Dermatol. 24 (2023) 225–245.
[9] A.L. Hung, M. Lim, T.L. Doshi, Targeting cytokines for treatment of neuropathic pain, Scand J Pain 17 (2017) 287–293.

[10] H. Iwata, C. Goettsch, A. Sharma, P. Ricchiuto, W.W. Goh, A. Halu, I. Yamada, H. Yoshida, T. Hara, M. Wei, N. Inoue, D. Fukuda, A. Mojcher, P.C. Mattson, A. L. Barabasi, M. Boothby, E. Aikawa, S.A. Singh, M. Aikawa, PARP9 and PARP14 cross-regulate macrophage activation via STAT1 ADP-ribosylation, Nat. Commun. 7 (2016) 12849.
[11] M.G. Jeschke, F.M. Wood, E. Middelkoop, A. Bayat, L. Teot, R. Ogawa, G. G. Gauglitz, Scars, Nat. Rev. Dis. Primers 9 (2023) 64.
[12] N. Keating, S.E. Nicholson, SOCS-mediated immunomodulation of natural killer cells, Cytokine 118 (2019) 64–70.
[13] W. Kim, D.Y. Kim, K.H. Lee, RNA-binding proteins and the complex pathophysiology of ALS, Int. J. Mol. Sci. 22 (2021).
[14] Y.J. Kim, J.H. Kim, K.J. Lee, M.M. Choi, Y.H. Kim, G.E. Rhie, C.K. Yoo, K. Cha, N. R. Shin, Botulinum neurotoxin type a induces TLR2-mediated inflammatory responses in macrophages, PLoS One 10 (2015) e0120840.
[15] H.J. Lee, Y.J. Jang, Recent understandings of biology, prophylaxis and treatment strategies for hypertrophic scars and keloids, Int. J. Mol. Sci. 19 (2018).
[16] K.W.A. Lee, L.K.W. Chan, A.W.K. Lee, C.H. Lee, J. Wan, K.H. Yi, Immunogenicity of botulinum toxin type a in different clinical and cosmetic treatment, a literature review, Life (Basel) 14 (2024).
[17] Y. Li, X. Shan, Q. Mao, R. Xiang, Z. Cai, Botulinum toxin type a intralesional monotherapy for treating human hypertrophic scar in a dose-dependent manner: in an animal model, J. Plast. Reconstr. Aesthet. Surg. 74 (2021) 3186–3195.
[18] Y.H. Li, J. Yang, Z. Zheng, D.H. Hu, Z.D. Wang, Botulinum toxin type a attenuates hypertrophic scar formation via the inhibition of TGF-beta1/Smad and ERK pathways, J. Cosmet. Dermatol. 20 (2021) 1374–1380.
[19] J. Mika, E. Rojewska, W. Makuch, M. Korostynski, S. Luvisetto, S. Marinelli, F. Pavone, B. Przewlocka, The effect of botulinum neurotoxin a on sciatic nerve injury-induced neuroimmunological changes in rat dorsal root ganglia and spinal cord, Neuroscience 175 (2011) 358–366.
[20] L. Moretti, J. Stalfort, T.H. Barker, D. Abebayehu, The interplay of fibroblasts, the extracellular matrix, and inflammation in scar formation, J. Biol. Chem. 298 (2022) 101530.
[21] T. Murakami, S. Shigeki, Pharmacotherapy for keloids and hypertrophic scars, Int. J. Mol. Sci. 25 (2024).
[22] M.J. O'Connor, T. Thakar, C.M. Nicolae, G.L. Moldovan, PARP14 regulates cyclin D1 expression to promote cell-cycle progression, Oncogene 40 (2021) 4872–4883.
[23] W. Qin, H.J. Wu, L.Q. Cao, H.J. Li, C.X. He, D. Zhao, L. Xing, P.Q. Li, X. Jin, H. L. Cao, Research Progress on PARP14 as a drug target, Front. Pharmacol. 10 (2019) 172.
[24] L.B. Schenkel, J.R. Molina, K.K. Swinger, R. Abo, D.J. Blackwell, A.Z. Lu, A. E. Cheung, W.D. Church, K. Kunii, K.G. Kuplast-Barr, C.R. Majer, E. Minissale, J. R. Mo, M. Niepel, C. Reik, Y. Ren, M.M. Vasbinder, T.J. Wigle, V.M. Richon, H. Keilhack, K.W. Kuntz, A potent and selective PARP14 inhibitor decreases protumor macrophage gene expression and elicits inflammatory responses in tumor explants, cell, Chem. Biol. 28 (2021) 1158–1168 e1113.
[25] S. Shakya, K. Asosingh, J.A. Mack, E.V. Maytin, Optimized protocol for the preparation of single cells from cutaneous wounds for flow cytometric cell sorting and analysis of macrophages, MethodsX 7 (2020) 101027.
[26] L. Shen, Y. Zhou, J. Gong, H. Fan, L. Liu, The role of macrophages in hypertrophic scarring: molecular to therapeutic insights, Front. Immunol. 16 (2025) 1503985.
[27] I. Sturniolo, C. Varoczy, Z. Regdon, A. Mazlo, S. Muzsai, A. Bacsi, G. Intili, C. Hegedus, M.R. Boothby, J. Holechek, D. Ferraris, H. Schuler, L. Virag, PARP14 contributes to the development of the tumor-associated macrophage phenotype, Int. J. Mol. Sci. 25 (2024).
[28] W. Wei, G. Zhao, Q. Li, J. Zhang, H. Wei, C. Shen, B. Zhao, Z. Ji, L. Wang, Y. Guo, P. Jin, Botulinum toxin type a alleviates androgenetic alopecia by inhibiting apoptosis of dermal papilla cells via targeting circ_0135062/miR-506-3p/Bax Axis, Aesth. Plast. Surg. 48 (2024) 1473–1486.
[29] H. Wu, A. Lu, J. Yuan, Y. Yu, C. Lv, J. Lu, Mono-ADP-ribosylation, a MARylationmultifaced modification of protein, DNA and RNA: characterizations, functions and mechanisms, Cell Death Discov 10 (2024) 226.
[30] F. Xu, W.Q. Cui, Y. Wei, J. Cui, J. Qiu, L.L. Hu, W.Y. Gong, J.C. Dong, B.J. Liu, Astragaloside IV inhibits lung cancer progression and metastasis by modulating macrophage polarization through AMPK signaling, J. Exp. Clin. Cancer Res. 37 (2018) 207.
[31] X. Xu, S. Gu, X. Huang, J. Ren, Y. Gu, C. Wei, X. Lian, H. Li, Y. Gao, R. Jin, B. Gu, T. Zan, Z. Wang, The role of macrophages in the formation of hypertrophic scars and keloids, Burns Trauma 8 (2020) tkaa006.
[32] M. Xue, C.J. Jackson, Extracellular matrix reorganization during wound healing and its impact on abnormal scarring, Adv Wound Care (New Rochelle) 4 (2015) 119–136.
[33] Z. Yang, Y. Lv, Z. Yang, L. Cao, D. Cao, Concentration-dependent inhibition of hypertrophic scar formation by botulinum toxin type a in a rabbit ear model, Aesth. Plast. Surg. 46 (2022) 3072–3079.
[34] M. Yuan, H. Shi, B. Wang, J. Cai, W. Yu, W. Wang, Q. Qian, Y. Wang, X. Zhou, J. Liu, Targeting SOCS2 alleviates myocardial fibrosis by reducing nuclear translocation of beta-catenin, Biochim. Biophys. Acta, Mol. Cell Res. 1871 (2024) 119804.
[35] F.L. Zhang, Z. Hu, Y.F. Wang, W.J. Zhang, B.W. Zhou, Q.S. Sun, Z.B. Lin, K.X. Liu, Organoids transplantation attenuates intestinal ischemia/reperfusion injury in mice through L-malic acid-mediated M2 macrophage polarization, Nat. Commun. 14 (2023) 6779.
[36] S.J. Zhao, F.Q. Kong, J. Jie, Q. Li, H. Liu, A.D. Xu, Y.Q. Yang, B. Jiang, D.D. Wang, Z.Q. Zhou, P.Y. Tang, J. Chen, Q. Wang, Z. Zhou, Q. Chen, G.Y. Yin, H.W. Zhang, J. Fan, Macrophage MSR1 promotes BMSC osteogenic differentiation and M2-like polarization by activating PI3K/AKT/GSK3beta/beta-catenin pathway, Theranostics 10 (2020) 17–35.
[37] N. Zhou, D. Li, Y. Luo, J. Li, Y. Wang, Effects of botulinum toxin type a on microvessels in hypertrophic scar models on rabbit ears, Biomed. Res. Int. 2020 (2020) 2170750.
[38] Z. Zhu, J. Ding, Z. Ma, T. Iwashina, E.E. Tredget, Systemic depletion of macrophages in the subacute phase of wound healing reduces hypertrophic scar formation, Wound Repair Regen. 24 (2016) 644–656.

作者简介：李建锐 中国创造学会创研委委员
中国妇幼保健协会医疗美容专业委员会常务委员
中华医学会整形外科学分会神经纤维瘤病学术工作组委员
中华医学会整形外科学分会躯干学术工作组委员
中国整形美容协会精准与数字医学分会理事
复旦大学外科学博士

投邮箱：zchjbtg@163.com

编辑：顾永毅 陆娴 曹冰峰 余杰
审编：孔令一
主审：郭鹏、郭强、陈洁、朱涛、项志康、陈霞
主编：刘宏建、林青、李信春、李喆
终审：李芹 张磊
素材收录时间：2025年6月1日-2025年6月30日

中国创造学会
2025年6月30日发